2004

Performance of singlemode fiber and Bragg grating due to bending and temperature

Thang Q. Tran
San Jose State University

PERFORMANCE OF SINGLEMODE FIBER AND BRAGG GRATING DUE TO BENDING AND TEMPERATURE

A Thesis

Presented to

The Faculty of the Department of Mechanical and Aerospace Engineering

San Jose State University

In Partial Fulfillment

of the Requirements for the Degree

Master of Science

By

Thang Q. Tran

August 2004

INFORMATION TO USERS

The quality of this reproduction is dependent upon the quality of the copy submitted. Broken or indistinct print, colored or poor quality illustrations and photographs, print bleed-through, substandard margins, and improper alignment can adversely affect reproduction.

In the unlikely event that the author did not send a complete manuscript and there are missing pages, these will be noted. Also, if unauthorized copyright material had to be removed, a note will indicate the deletion.

ProQuest Information and Learning Company
300 North Zeeb Road
P.O. Box 1346
Ann Arbor, MI 48106-1346

APPROVED FOR THE DEPARTMENT OF MECHANICAL AND AEROSPACE ENGINEERING

Dr. Fred Barez, Committee Chair

Dr. Raymond Yee, Committee Member

Dr. Nicole Okamoto, Committee Member

APPROVED FOR THE UNIVERSITY

ABSTRACT

PERFORMANCE OF SINGLEMODE FIBER AND BRAGG GRATING
DUE TO BENDING AND TEMPERATURE

By Thang Tran

Characteristics of performance degradation of singlemode fiber and Bragg grating due to bending stress and temperature effects are studied. The optical parameters that are observed in the study are attenuation, dispersion, and birefringence effect in polarization. The significant factor that bending stress and temperature have on the light transmission is their effects on the index of refraction of fused silica fiber and grating parameter. The increase in stress in the core of the fiber would result in the decrease in the index of refraction, and the increase in temperature would result in the decrease in refractive index of fused silica. The attenuation, waveguide dispersion, and birefringence in singlemode fiber are all found to increase with the decrease in refractive index value. The temperature effect on the change of index of refraction results in negligible levels of attenuation, dispersion, and birefringence. Fiber Bragg grating strain sensitivity is increased with larger change in index of refraction, and is more sensitive at higher wavelengths. The grating sensitivity is about 8 times higher to temperature than strain effect.

ACKNOWLEDGEMENTS

I would like to express my greatest appreciation toward my research advisors, Dr. Fred Barez, Dr. Nicole Okamoto, and Dr. Raymond Yee, for all the support and guidance for this research. I would also like to thank Dr. Kevin Sawyer for many useful discussions and comments concerning the finite element modeling ideas that help to provide more insights into approaching the problem with Abaqus. My gratitude also goes to many friends who spend many hours helping with the reading and giving feedback to this paper.

I would like to especially thank my family for much of the support and patient over this time, without whom, this thesis would not be possible.

Dedicated to Mom, Dad, and Florie

TABLE OF CONTENTS

LIST OF TABLES

Table **Page**

LIST OF FIGURES

Figure **Page**

Figure **Page**

Figure **Page**

Figure **Page**

CHAPTER 1

Introduction

1.1 Fiber optics and applications

In the age of the Internet revolution, the demand for a faster and better way of communication is ever increasing. As more streaming data traffics through the network, the capacity of the network has to increase to handle this demand. The legacy network of copper technology has made many improvements in itself, but it is still limited to how fast the electron can travel through the network. A new approach using photonics technology comes to life to meet this speed and bandwidth demand of modern communication network, as more and more applications and businesses are handled through the Internet.

The photonics technology enables information to be transferred from one location to another by light traveling over the optical fiber carrying the digital data. The data rate here is the speed of many photons traveling in a medium of the optical fiber, where fused silica glass is commonly used for telecommunication networks. The simple structure of the photonic network is composed of a light source, typically a laser source that is coupled to the optical fiber, and the electronics that are used to convert digital signal to optical signal and back. The more complex photonic network can have additional optical amplifiers and detectors to maintain signal conditioning over a long haul system, where it is prone to more signal degradation due to the longer distance that light has to travel. The laser source can operate at a single wavelength or multiple wavelengths. The latter case can be seen in application of the tunable laser source where there is flexibility of

wavelength adjustment to provide a high bandwidth for data. In a telecommunication system, the common wavelength range of use is from 1525 to 1575 nanometers. This is recognized as C-band in physics of optics.

The optical fiber is the element that has a significant role in determining the system characteristic of data transmission, in terms of system performance. Singlemode fiber is widely used in modern telecommunication networks. It is chosen because it allows only one light wave of optical signal to travel in the fiber at a time. This helps to reduce the problem of having many wavelengths at the receiving end such as in a multimode fiber. However, the singlemode fiber can be very sensitive to external disturbances like residual stress due to bending and temperature change. These effects can introduce power loss, change in polarization, change in beam profiling, and noise. The result would be the loss of data signal and a noisy system. It is thus important to study and understand these effects on the fiber, primarily in areas of stress-induced and temperature effects on signal quality of a singlemode fiber.

1.2 Singlemode fiber and Bragg grating

Optical fibers shown in the Figure 1 are those of singlemode and multimode fibers. There is a central core, within which the light field propagates, which is surrounded by a cladding layer, and in turn is surrounded by a protective jacket, and also perhaps with one or two outer protective jackets. The mode in fiber can be thought of as a pattern of standing wave that the field pattern forms on the cross section of the fiber. If there are many such standing waves across the fiber core diameter, the fiber is operating

in multimode; and if there is only one it is operating in singlemode fashion. The core and cladding material are made of low loss fused silica glass, and the jackets are made of plastic or polyurethane materials. The color coding on the outer buffer of fibers are yellow for singlemode and orange for multimode fibers, for which one may have seen fiber cables being run within buildings.

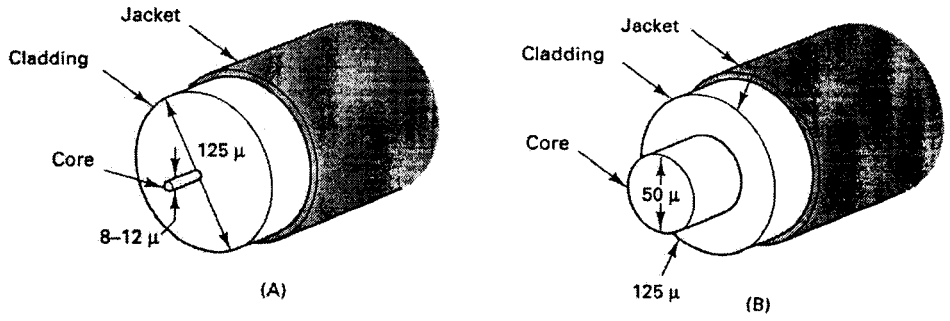

Figure 1. Geometry of (a) singlemode and (b) multimode optical fibers [1].

A singlemode fiber typically has the design geometry of that shown in the figure above. The core is made of fused silica glass and has a diameter of about 8-12 um. The cladding on the other hand has a diameter of 125 um and is also made of fused silica glass. In order to minimize the loss of light absorbed or escaped in the radial direction, the silica glass index of refraction for the core has to be higher than that of the cladding. This principle is called the total internal reflection [2]. In order for light transmission to work, light within the core has to be reflecting back to the core when hitting the boundary of core and cladding materials. The significance here is that the fused silica glass index

of the core has to be higher than that of the cladding, which is also made of fused silica glass. The design relationship for singlemode fibers with step index structure is shown:

$$2\pi a/\lambda \, [\mathrm{sqrt}(n1\text{^}2-n2\text{^}2)] = 2.4$$

Here, n1 is the core index, n2 is the cladding index, a is the core radius, λ is the operating wavelength, and "2.4" is the cutoff definition for singlemode fiber [3]. This relationship determines the core radius geometry for certain indices of refraction between the core and the cladding, for an operating wavelength.

Recent technology has been showing promises of real time monitoring of structural integrity by using surface mounted optical fiber strain gauges. In some engineering applications, there is an advantage in having small strain gauges to measure localized strain.

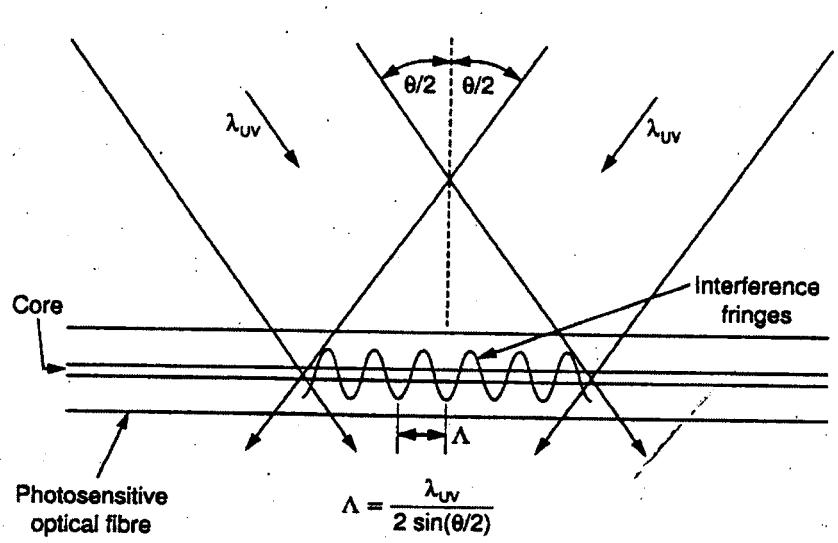

Figure 2. Inscription of a periodic grating in the core of Fiber Bragg grating [6].

Fiber Bragg grating (FBG) sensors are well fit for these applications, not only just suitable for measuring strain, but pressure and temperature as well [4, 5]. Fiber Bragg grating is a periodic grating that its pattern is being inscribed in the core of the photosensitive fiber by two interfering UV beams at wavelength λ_{uv}. Figure 2 shows the layout of such fabrication technique and details of theoretical background is shown in the tutorial review by Bennion et al [6].

The wavelength of the reflected wave is governed by the grating constant or period L and the refractive index of the fiber n by the Bragg reflection condition:

$$\lambda_{BO} = 2nL$$

where λ_{BO} is the Bragg wavelength at room temperature and free of stress. As the fiber undergoes through external shear stress, the Bragg grating planes that are inscribed onto and along the fiber core surface will be sheared through a small angle φ, which is shown in Figure 3.

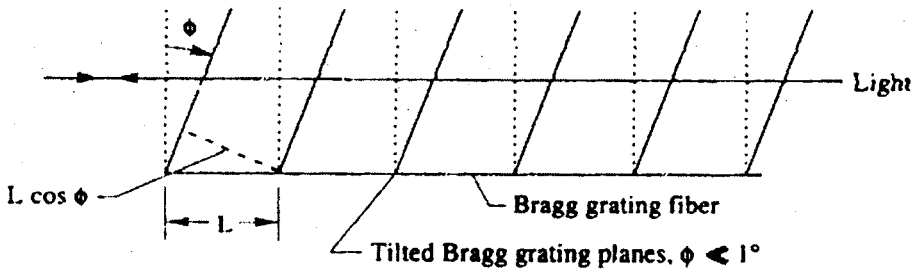

Figure 3. Schematic diagram of shear stress grating [7].

The change in Bragg wavelength is defined by Parmar [7] as follow:

$$\Delta\lambda_B = \Delta\lambda_{BT} + \Delta\lambda_{BS}$$

where $\Delta\lambda_{BT}$ is the temperature induced shift of wavelength, and $\Delta\lambda_{BS}$ is the stress induced shift in Bragg wavelength. The temperature induce shift is related to index of refraction as:

$$\Delta\lambda_{BT} = (d\lambda_B/dT)\Delta T$$

and $\lambda_B = 2nL$

Thus $\Delta\lambda_{BT} = 2nL^* \Delta T$

The shear induced Bragg wavelength change is defined as follow:

$$\lambda_{BS} = 2nL^*[(\Delta L/L)^*(1+\Delta n/n)+\Delta n/n]$$

Here $\Delta n/n$ is small and $\Delta n/n << \Delta L/L << 1$

Thus, it can be approximated as:

$$\lambda_{BS} = 2nL^*(\Delta L/L) = 2nL^*\varepsilon(R)$$

where $\varepsilon(R)$ is the strain induced resulting from the bending of fiber and is the function of

bending radius.

1.3 Attenuation in optical fibers

The phenomenon where optical signal travels though a medium and experiences a loss in power is defined as attenuation. As the signal propagates through a fiber, the optical power loss will eventually attenuate the signal until it is lost in noise at the receiver. For a telecommunication system, it is of our interest to understand the mechanism of this loss and determine an optimum operating wavelength that has a lowest attenuation and dispersion.

The model for power loss of optical signal inside the fiber can be shown as follow:

$$P_t = P_o \exp(-\alpha L)$$

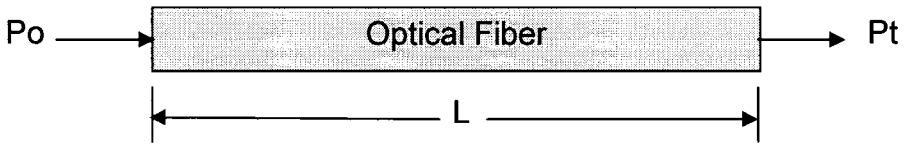

Figure 4. Attenuation model in optical fiber.

where P_t is the transmitted power, P_o is the power launched at input, L is length of fiber, and α is the attenuation constant. It is customary to express the fiber loss in units of decibels per kilometer (dB/km), where this constant is represented by α, and is related to the attenuation constant as follow:

$\alpha = -10/L \log(Pt/Po) = 4.343\alpha$

The fiber loss is depending on the wavelength of light. Figure 5 shown by Agrawal the loss of a singlemode fiber made using the modified chemical vapor deposition (MCVD) process. The fiber exhibits a minimum loss about 0.2 dB/km near 1550 nm wavelength. Note that in modern telecommunication system, the chosen operating wavelength is in the middle of C band wavelength range at 1550 nm, shown in Figure 5, since it is near the lowest attenuation factor for singlemode fiber. It is noticeable that the loss is much higher at lower wavelength, reaching 1-10 dB/km in the visible region. It is, however, even within the 10 dB/km loss regime, it is still corresponding to the attenuation constant of α=2E-5 /cm, which is a truly low value of loss for silica glass comparing to other materials [8].

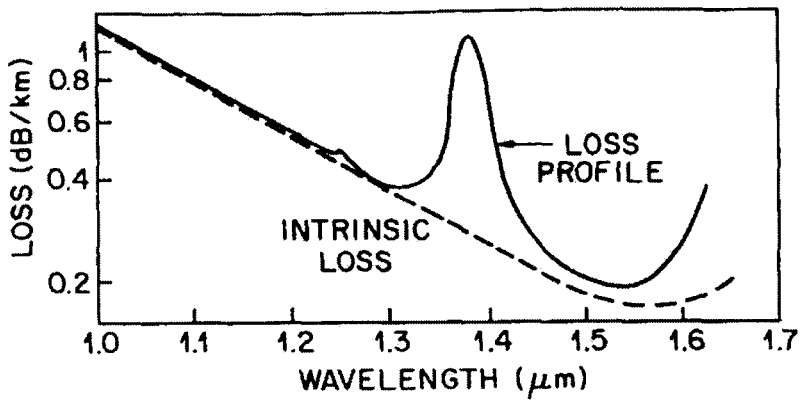

Figure 5. Measured loss profile characteristic of singlemode fiber [8].

Note that the two peaks at about 1230 nm and 1370 nm on the loss profile are due to OH-

absorption, where it is resulting from hydrogen interaction with the glass to produce hydroxyl ions and their losses. This is caused when the fiber is exposed to hydrogen gas, which can be produced by corrosion of steel strength members or bacteria. The solution can be to add a coating to the fiber to protect it against hydrogen absorption [9].

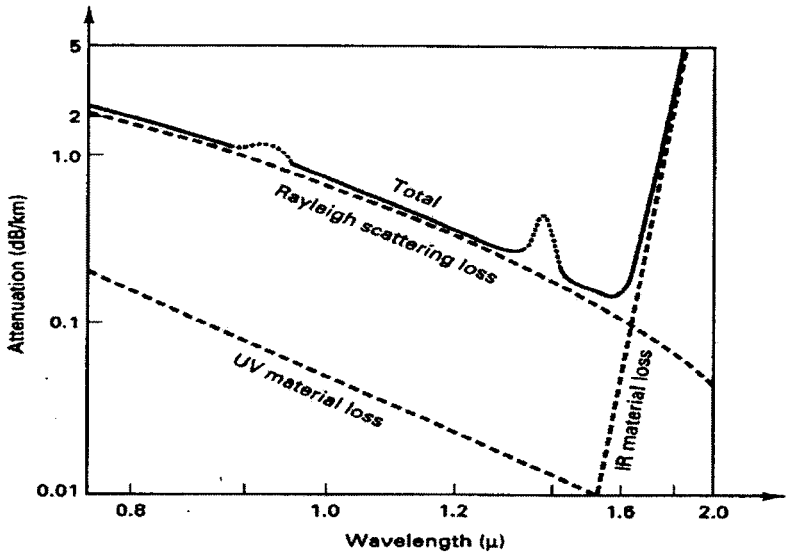

Figure 6. Spectra of three kinds of attenuation in silica fibers [10].

To take another closer look at attenuation in fibers, it is important to understand the combined effect of attenuation loss and those of other physical phenomenon. There are three kinds of fiber attenuation in silica fibers. They are UV material loss, IR material loss, and Rayleigh scattering loss, and they all do contribute to overall loss spectrum. Figure 6 shows that the loss due to UV material loss is significant at lower wavelengths, and it drops off at about 1500 nm, which is also the lowest and starting point of the IR material loss curve. The IR material loss is increasing with long wavelength region, where the absorption loss spectrum consists of peaks out beyond

9000 nm with attenuation of over 10 dB/km [10]. The Rayleigh scattering loss is decreasing as wavelength increases, and it is the most significant in overall loss spectrum from lower wavelengths to about 1500 nm. In silica fibers, density and glass compositional non-uniformity contribute to scattering loss, and they are frozen into glass during manufacture. Scattering wastes energy by misdirecting it away from the desired propagation direction along the fiber axis.

Since singlemode optical fibers are promising transmission media for long distance broadband transmission, it is therefore important to evaluate the attenuation property of such. It is well known that dielectric waveguides lose power by radiation if their axes are bent. Many authors have studied the issue with many approaches and assumptions. Lewin solved the problem by constructing a solution for electromagnetic field [11]. Snyder and White had derived the curvature loss formula of the slab and of the fiber by using the field of the straight fiber as a first approximation in the diffraction integral in it vector form [12]. Chang and Kuester applied a technique of calculation of radiation loss on an arbitrary curved surface-wave structure for transverse electric or TE mode, which does not have a component of the electric field in the direction of wave propagation, of slab waveguide and for all modes of curve optical fiber [13].

The most direct derivation of radiation loss for optical fiber had been done by Marcuse [14], by considering the waveguide in cylindrical polar coordinate system and looking at the field solution outside of the slab and in the infinite cladding, solution must be a simple Hankel function. Figure 7 shows the core geometry with index of n1 and cladding index n2 in the bent profile. The derivation involves elaborate mathematics, and

details are reserved for the reference by Marcuse.

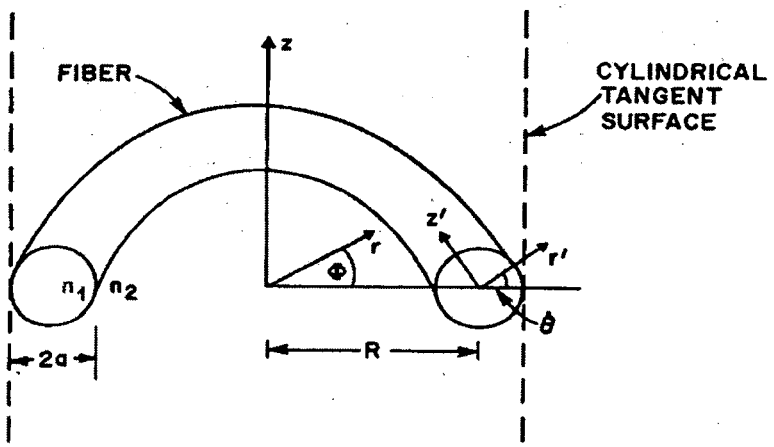

Figure 7. Fiber bend model with bending radius R [14].

The curvature loss formula is shown as follow:

$$2\alpha = \frac{\sqrt{\pi}\kappa^2 \exp[-\frac{2}{3}(\gamma^3/\beta_g^2)R]}{2\gamma^{3/2}V^2\sqrt{R}(\ln\gamma a)^2} \qquad [14]$$

where (2α) is the curvature loss or attenuation coefficient due to bending in dB/km, a is the core radius, and R is the bending radius. The other parameters are defined as follow:

$\kappa = (n1^2k^2-\beta g^2)^{\wedge}1/2$

$\beta g = nk$ (where $n1k < \beta g < n2k$)

$\gamma = (\beta g^2-n2^2k^2)^{\wedge}1/2$

$$V^2 = k^2a^2(n1^2-n2^2)$$

And $k = 2\pi/\lambda$

Here, βg is the Propagation Constant and k is the wave number in free space, which is a function of wavelength. For the purpose of derivation of 2α above and of this work, it is assumed that the operation of singlemode fiber belongs to category of Weakly Guiding Fibers [15], where the difference between the index of refraction of the core and cladding, Δ, is small. It is assumed in this study that Δ equals to 0.2% (or 0.002) because the model is assumed to be weakly guiding model and is a commonly accepted value when building long distance and high data rate optical system [16]. The mode of operation is also assumed to be in linearly polarized (LP) modes, where light polarization is resulted into x and y components of the electric field only. Note that LP01 is equal to HE11 mode for weakly guided modes. The role of n in βg where $n1k<\beta g<n2k$ is relevant because when n is close to n1, it represent high field in the core, and when n is close to n2 it is near cutoff region of the field in the core. It is assumed that there is minimal loss due to other factor like Rayleigh scattering, thus n is of 99.9% of n1 for light propagation in fiber.

1.4 Dispersion in optical fibers

Optical fibers are usually characterized by two important parameters: loss and dispersion. Attenuation or loss determines how far the signal can travel before it requires regeneration. Dispersion, on the other hand, is used to describe the tendency of the fiber

to distort the light pulse when traveling though it. In general, dispersion is observed with distance and bandwidth. If length is short, the signal bandwidth that can be transmitted is very large. With increasing length, the signal distortion becomes more severe so that the desired channel capacity limits the length the signal can be transmitted through fiber without regeneration. There are many different causes of dispersion in fibers, of which the most significant are material dispersion, waveguide dispersion, and modal dispersion. Modal dispersion is often referred to as group delay and it is caused by the difference in path lengths that are associated with each of the modes of the fiber [17]. It is important for multimode fibers because it shows the delay time between the fast and slow propagation modes. In singlemode fibers, it is not a factor of concern and thus not being discussed here.

Dispersion in singlemode fibers are caused mainly by the dispersive properties of the material. This is called the material dispersion or chromatic dispersion, where the light energy of the pulse traveling in a singlemode fiber is spread out over a certain spectral range, partly due to the Fourier spectrum associated with the signal pulse, but also because the light source itself has a broad spectral width even before modulation [18].

In a homogeneous non-dispersive medium, the light propagates at a velocity V_p, called the phase velocity. When the medium is dispersive, the phase velocity V_p becomes a function of wavelength, and the signal must have a nonzero bandwidth, where upon the dispersion enters the picture, in order to send information in real life application. The phase velocity V_p is observed as a phase front velocity of light propagation, where as

the group velocity, V_g, is the actual velocity that the information is transmitted [19].

When an electromagnetic wave interacts with electrons of a dielectric of fiber, the medium response generally depends on the optical frequency ω. This is referred to as chromatic dispersion and shown through the frequency dependence of the refractive index $n(\omega)$. To account the effect of fiber dispersion, the mode propagation constant, β, in Taylor series is expanded about the frequency ω_o:

$$\beta(\omega) = n(\omega)\frac{\omega}{c} = \beta_0 + \beta_1(\omega-\omega_0) + \frac{1}{2}\beta_2(\omega-\omega_0)^2 + \cdots$$

where

$$\beta_m = \left[\frac{d^m\beta}{d\omega^m}\right]_{\omega=\omega_0} \quad (m = 0, 1, 2, \ldots).$$

[20]

The resulting parameters $\beta 1$ and $\beta 2$ are determined by Agrawal in 1989 [20]. The $\beta 1$ relates to pulse envelop moving group velocity, and $\beta 2$ is responsible for pulse broadening. These parameters relate to the refractive index n and its derivatives through the relations:

$$\beta_1 = \frac{1}{c}\left[n + \omega\frac{dn}{d\omega}\right] = \frac{n_g}{c} = \frac{1}{v_g},$$

$$\beta_2 = \frac{1}{c}\left[2\frac{dn}{d\omega} + \omega\frac{d^2n}{d\omega^2}\right] \simeq \frac{\omega}{c}\frac{d^2n}{d\omega^2} = \frac{\lambda^3}{2\pi c^2}\frac{d^2n}{d\lambda^2}.$$

[20]

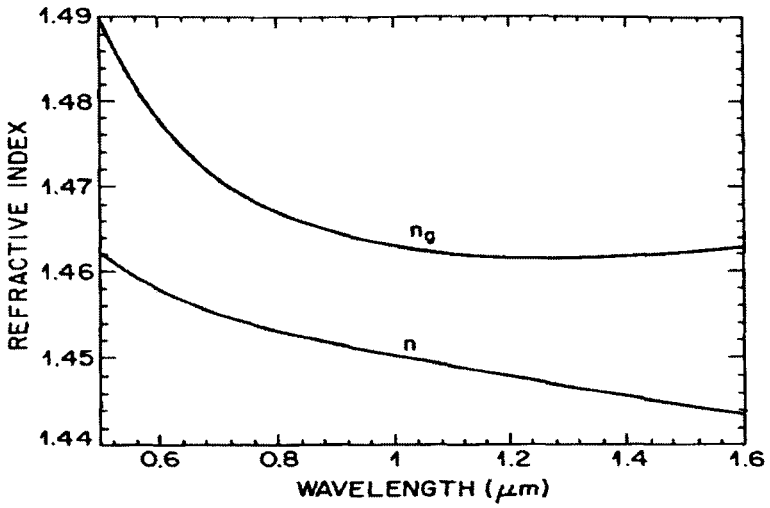

Figure 8. Variation of refractive index n and group index n_g with wavelength for fused silica [20].

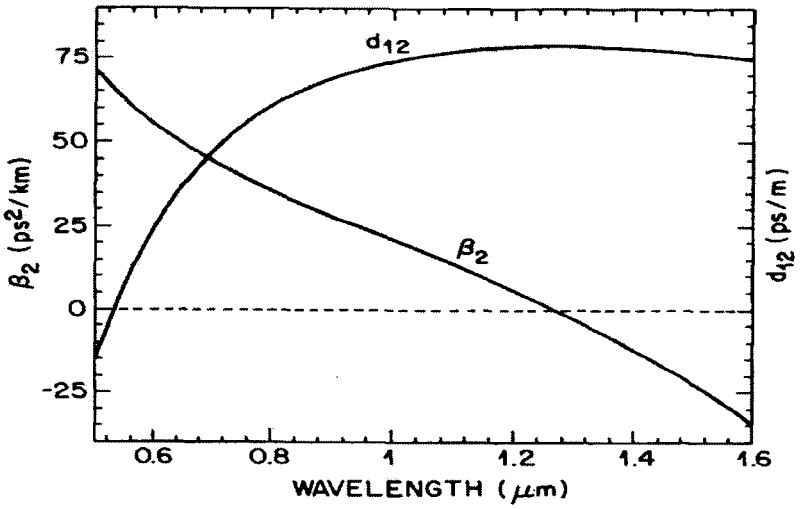

Figure 9. Variation of β_2 and d_{12} with wavelength for fused silica [20].

Figures 8 and 9 show the variation of n, n_g, and β_2 with wavelength λ for fused silica. The most important feature to notice is that the parameter β_2, which is the group velocity dispersion parameter, vanishes at wavelength of 1270 nm, and it becomes negative for longer wavelengths. The wavelength at which $\beta_2 = 0$ is referred to as the

zero-dispersion wavelength λ_D. The curves in Figures 8 and 9 are for bulk fused silica.

The dispersion behavior for glass in optical fibers generally deviates from that shown in the figures for two following reasons. First, the fiber core may have small amount of dopants such as GeO2 and P2O5. Second, because of the dielectric waveguiding or light traveling on an optical medium, the effective mode index is slightly lower than the material index n(ω) [21]. This results in a waveguide contribution that must be added to the material contribution to get the total dispersion effect in fiber. Figure 10 shows the measured total dispersion of a singlemode fiber. The plotted dispersion parameter, D, which is commonly used in fiber optics literature, relates to the group velocity dispersion parameter, β2, as follow:

$$D = \frac{d\beta_1}{d\lambda} = -\frac{2\pi c}{\lambda^2}\beta_2 = -\frac{\lambda}{c}\frac{d^2 n}{d\lambda^2} \quad [21]$$

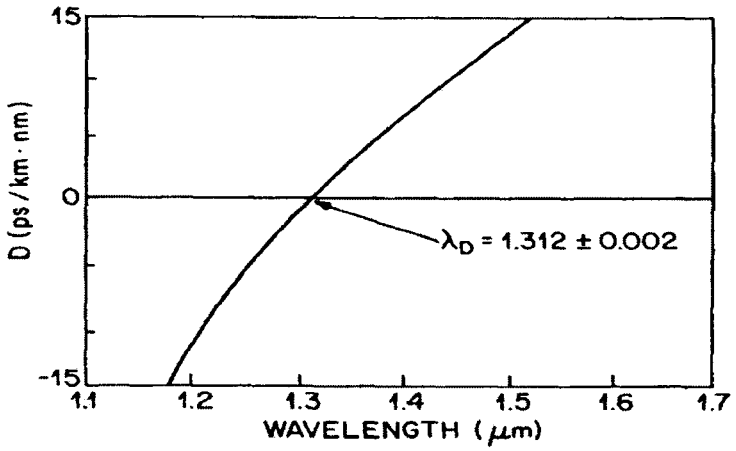

Figure 10. Measured total variation dispersion parameter D [21].

One feature of waveguide dispersion that is interesting is that its contribution to D (or $\beta 2$) depends on the fiber design parameters, like core radius a, and the core-cladding index difference Δ. This feature can be used to shift the zero dispersion wavelength λ_D close to 1550 nm, where it is also the wavelength with the smallest attenuation in fiber. This is of interest for optical telecommunication system build, because it is always a desired parameter to have the lowest attenuation and dispersion at the operating wavelength.

In calculating the material dispersion and waveguide dispersion in singlemode fibers, it is simpler to group terms together and plots some parameters together to show the dispersion relationships. Similarly, Powers [22] relates material dispersion with the quantity of $(\Delta\tau_{mat}/L\Delta\lambda)$ as the parameter D and group together the term $(\lambda^2 d^2n/d\lambda^2)$. The result is shown in Figure 11 as function of λ. The material dispersion is shown as:

$$(\Delta\tau_{mat}/L\Delta\lambda) = - (1/C\lambda) (\lambda^2 d^2n/d\lambda^2)$$

Note that the term $(\Delta\tau_{mat}/L\Delta\lambda)$ has a unit of picoseconds per kilometer per nanometer (ps/km*nm), which is the same as those of parameter D. Here, C is the speed of sound in vacuum of 3.0E8 m/s. Similarly, waveguide dispersion is shown as $(\Delta\tau_{wg}/L\Delta\lambda)$:

$$(\Delta\tau_{wg}/L\Delta\lambda) = - (n_2\Delta/C)*(1/\lambda)*(V\, d^2(Vb)/dV^2)$$

where n2 is the index of refraction of the cladding, and ($V\, d^2(Vb)/dV^2$) is grouped and shown by the plot (see Figures 12 and 13). It should be recognized that:

$$V = (2\pi a/\lambda)*(n1\sqrt{2\Delta})$$

V is the parameter that is used to determine of propagation mode. For step-index singlemode fibers, if $V < 2.405$, then only the first mode of propagation LP01 will propagate [23]. The notation LP is referred to as linearly polarization mode, where the first index "0" is the integer that enters the circular functions of sine and cosine in the transformation of the general vector field, and the second index "1" is used to label the root of the field solution [24].

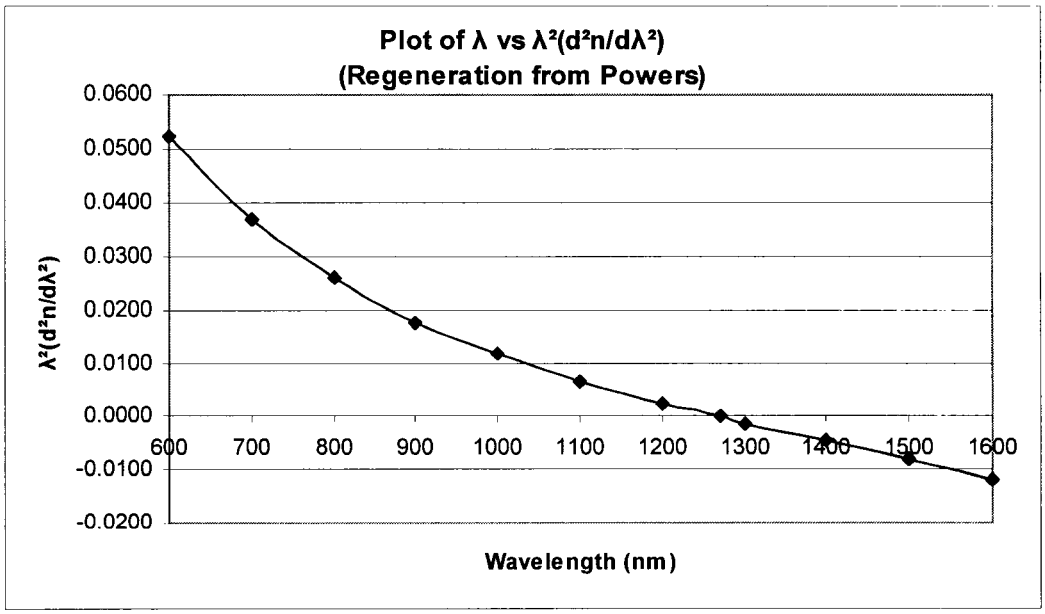

Figure 11. Regeneration of $\lambda^2(d^2n/d\lambda^2)$ and λ.

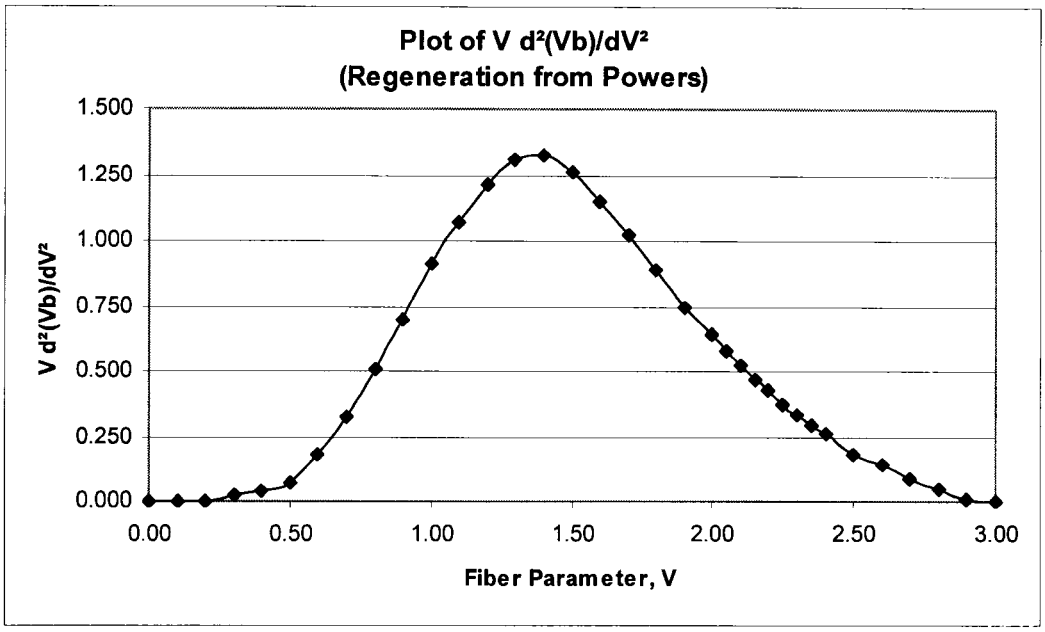

Figure 12. Regeneration of ($V\ d^2(Vb)/dV^2$) and Parameter V, Full Range.

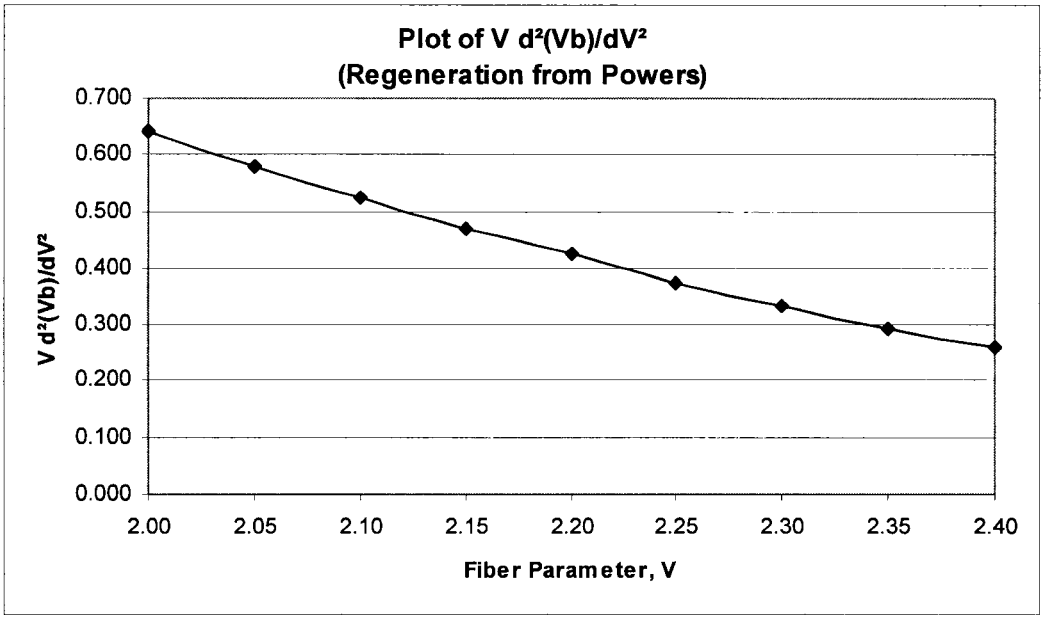

Figure 13. Regeneration of ($V\ d^2(Vb)/dV^2$) and Parameter V, for $2.0<V<2.4$.

1.5 Polarization and birefringence in optical fibers

Polarization in fiber is an important phenomenon to understand since it relates closely to the intensity of light and birefringence in singlemode fiber. Birefringence by definition is the refraction of light in an anisotropic material in two slight different directions to form two rays. It is observed with Maxwell's view that light is an oscillating magnetic field with the same frequency but oriented perpendicular to the electric field. The amplitude of the electric field in Figure 10 can be written as:

$$E(z,t) = Ex^{o}\sin(2\pi\nu t - 2\pi z/\lambda + \varphi o)$$

where ν is the frequency of the light wave, λ is the wavelength, Ex^{o} is the maximum amplitude, and φo is a constant specifying its absolute phase. The frequency is often expressed in circular frequency, $\omega = 2\pi\nu$, and the wavelength as a wave number, $k = 2\pi/\lambda$. Thus, another way to represent this in circular frequency and the wave number is:

$$E(z,t) = Ex^{o}\sin(\omega t - kz + \varphi o)$$

The electric field can also be used to express the energy density, U, and the intensity of light, I, as follow:

$$U(z,t) = 1/4\pi\ (E(z,t))\text{^}2$$

And $I = ((Ex^{o})\text{^}2)\lambda\nu/(8\pi)$

Figure 14 shows the light's oscillatory nature of orthogonal electric and magnetic field vectors; with (a) showing the spatial dependence of wave some point in time, and (b) showing the temperal dependence of waves passing some point in space [25].

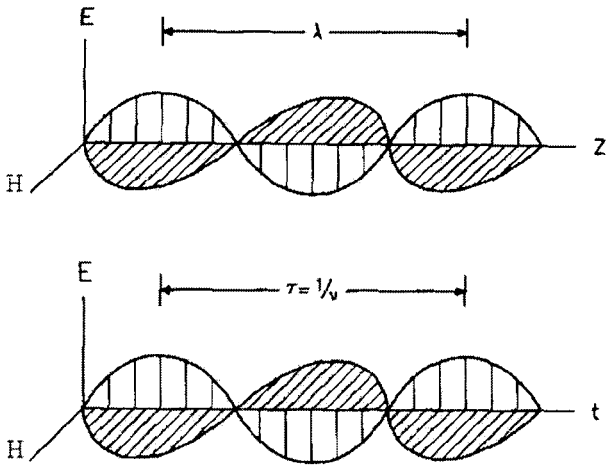

Figure 14. Light wave with oscillatory nature of orthogonal electric and magnetic field vectors [25].

A typical singlemode fiber will propagate with two fundamental modes with orthogonal polarizations. The difference in propagation constants of x and y direction, $(\beta x-\beta y)$, defines the modal birefringence. This modal birefringence is represented as B, where

$$B = (\beta x - \beta y)/(2\pi/\lambda) = \lambda/L$$

λ is the wavelength and L is the beat length. For a nominally circular fiber, B=10E-5 to 10E-6 and with special care, B can be as small as 10E-9. High birefringent fibers can

maintain a given mode of linear polarization over longer distance, where low birefringent fibers can maintain polarization and allow the observation of Faraday rotation by magnetic field, with no external perturbation allowed [26].

Birefringence is also sensitive to external disturbances such as bends and lateral stress. Such applications can be found in interferometric force sensing via fiber tension bending work done by Fürstenau [27]. Bending induced birefringence is described by:

$$\beta_b = (1/2)*C_s*(r/R)^2$$

where β_b is the birefringence due to bending effect, r is the fiber radius, and R is the fiber bend radius. C_s is the strain-optic coefficient, which is defined as follow:

$$C_s = 0.5k*(n\text{^}3)*(p_{11}-p_{12})*(1+\nu)$$

Here, $k = 2\pi/\lambda$, which is the wave number in free space, n is the index of refraction of fiber core, ν is the Poisson ratio, and p_{11} and p_{12} are the strain optic tensor constants in the y and z direction, or in the normal and parallel direction of light propagation. If the bend is due to a transverse force, a tension component of birefringence, β_{tc}, has to be added to β_b to get the total birefringence. β_{tc} is defined as:

$$\beta_{tc} = C_s*(2-3\nu)/(1-\nu)*(r/R)*\varepsilon_z$$

where ε_z is the coaxial strain, which results from the transverse tension force. In general for singlemode fibers, the birefringence $\Delta\beta=0$ represents a perfect fiber and $\Delta\beta=10$ deg/m (or 0.175 rad/m) is for a fiber with excellent circularity, given by Okoshi and Kikuchi [28].

1.6 Index of Refraction and Photoelasticity

The phenomenon where a glass fiber is under bending stress is investigated to understand its effect on loss of performance or light signal. When a glass is stressed in tension, it assumes the optical properties of a positive uniaxial crystal, where the optic axis is parallel to the axis of stress. The degree of birefringence, however, is not fixed, but is proportional to the stress, up to the limiting stress of glass. The proportionality constant between birefringence and stress is called the stress-optical coefficient [29].

The value for the stress-optical coefficient is influenced by the composition of glass, and some values are listed on Table 1, with units of pounds per square inch per millimicron per inch.

Material Type, Glass	Stress-Optical Coefficient (lbf/in² per milli-um*in)
Fused Silica	1.64
Plate	2.13
Sheet	2.31
Aluminosilicate	2.17

Table 1. Stress-optical coefficient for selected glass compositions.

The mechanism of stress optical effect has been interpreted by Mueller [30], that

straining of elastic solid produces two effects on the atomic level. The first is the increase in the spacing of the atoms in the direction of stress, and the other effect is the distortion of the atoms themselves. The former is called "lattice effect" and the later is referred to as the "atomic effect." Figure 15 is shown to illustrate this phenomenon.

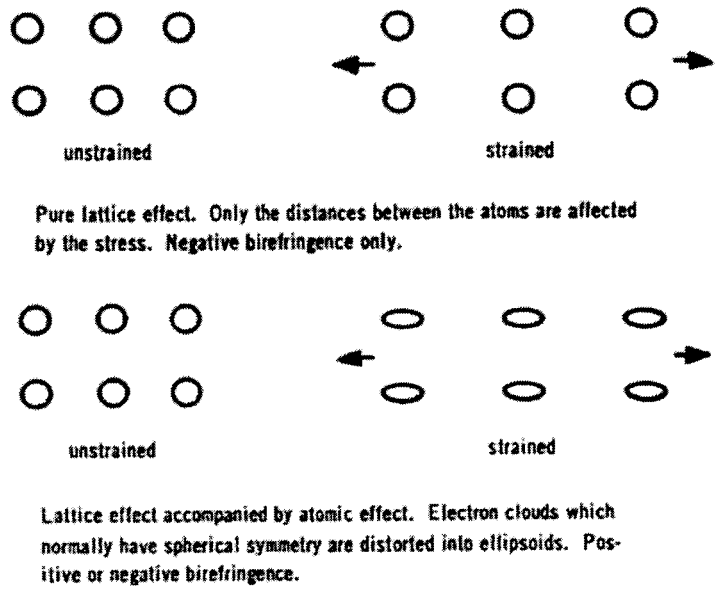

Figure 15. Illustration of lattice effect and atomic effect on silica atoms [29].

The lattice effect always produces negative sign birefringence, because an electric field that vibrates parallel to the strain axis sees a lower concentration of electrons than does an electric field vibrating perpendicular to this axis. Thus the ordinary light ray experiences more retardation than does the extraordinary ray. This is seen as $n_e < n_o$, and the birefringence is negative. In light transmission through crystals, the light component that travels through the crystal without deviation and obeys the laws of refraction is

called the ordinary ray, and the light component that deviates in the crystal and experiences the lateral displacement on emergence and does not obey Snell's law is called extraordinary ray [31].

On the other hand, the atomic distortion effect contributes to positive birefringence. It increases the concentration of electrons that encountered by extraordinary ray and decreases the concentration encountered by the ordinary ray.

The overall effect resulting of these positive and negative contributions is usually a positive sign of birefringence for isotropic material under tension condition [32]. This shows that the atomic effect becomes more significant than the lattice effect, where the glass becomes uniaxial positive under stress and negative under compression.

Index of refraction of glass relates to the stress-optical constants is shown by Shand [33] as follow:

$$n_l = n_o + C_1\sigma$$

And $$n_t = n_o + C_2\sigma$$

Where n_l and n_t correspond to incident light polarized in the parallel and perpendicular, respectively, to the fiber axis, n_o is the refractive index of the unstressed fiber, and C_1 and C_2 are stress optical constants associated with direct and transverse components. For pure bending condition, only C_2 is being considered, since C_1 is of negligible value in such case. Using the relative stress optical constant B, the relationship represents the total effect of index change and it takes the form as shown:

$$B = C_1 - C_2$$

Thus, $\Delta n = (n_1 - n_o) = B\sigma$

For fused silica, Primak and Post [34] obtained experimental data shown in Table 2 below. Their findings from other types of glass indicate that oxygen ions of fused (vitreous) silica are more deformable then the oxygen ions of other siliceous glasses and the thermal dilatation of the oxygen ion in the glasses would seem related to its strained bond configuration. These data for B and C_2 are fitted with Log functions over the data range of 436nm to 644nm, and interpolations based on the logarithmic functions are made for different wavelengths of interest, from 600nm to 1600nm. The results are shown in the Figure 16, 17, and 18. Note that both values of B and C_2 are positive, so that when the stress condition is in tension, the refractive index decreases as the result; compressive stresses increase the index of refraction value. This is consistent with the sign and the convention of that of Morey's finding [35].

Wavelength (nm)	Stress-optical Constant, B (d/cm²)^-1	Stress-optical Constant, C2 (d/cm²)^-1
436	3.66E-13	4.32E-13
546	3.56E-13	4.22E-13
579	3.54E-13	4.21E-13
589	3.53E-13	4.20E-13
644	3.51E-13	4.19E-13

Table 2. Stress-optical constants of fused silica for some chosen wavelengths.

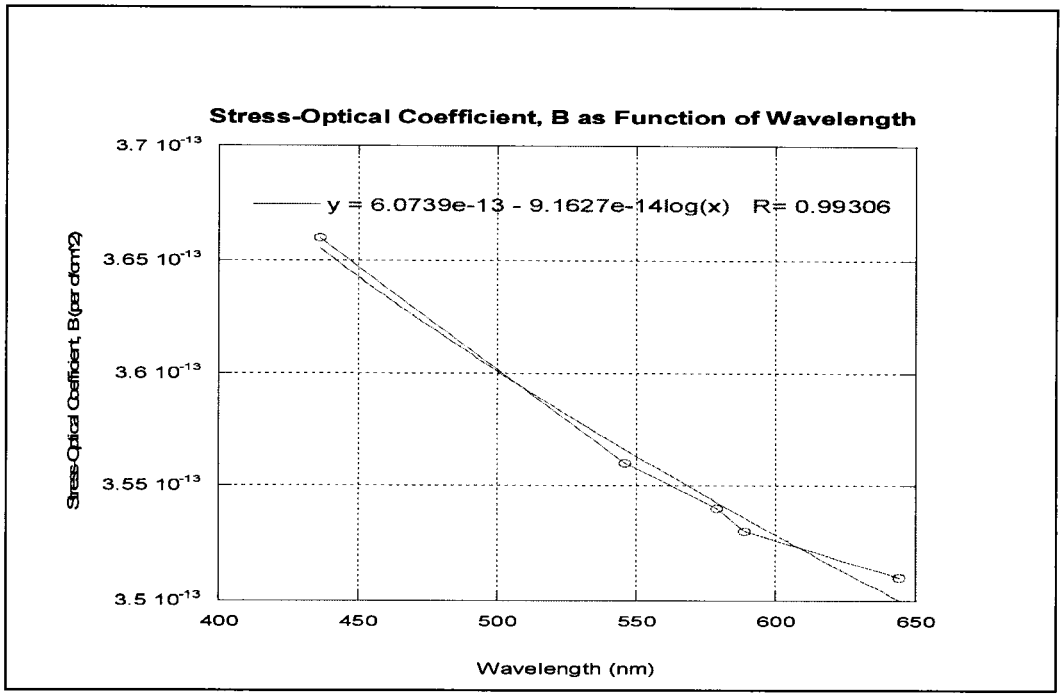

Figure 16. Fit data for stress optical coefficient B as function of wavelength.

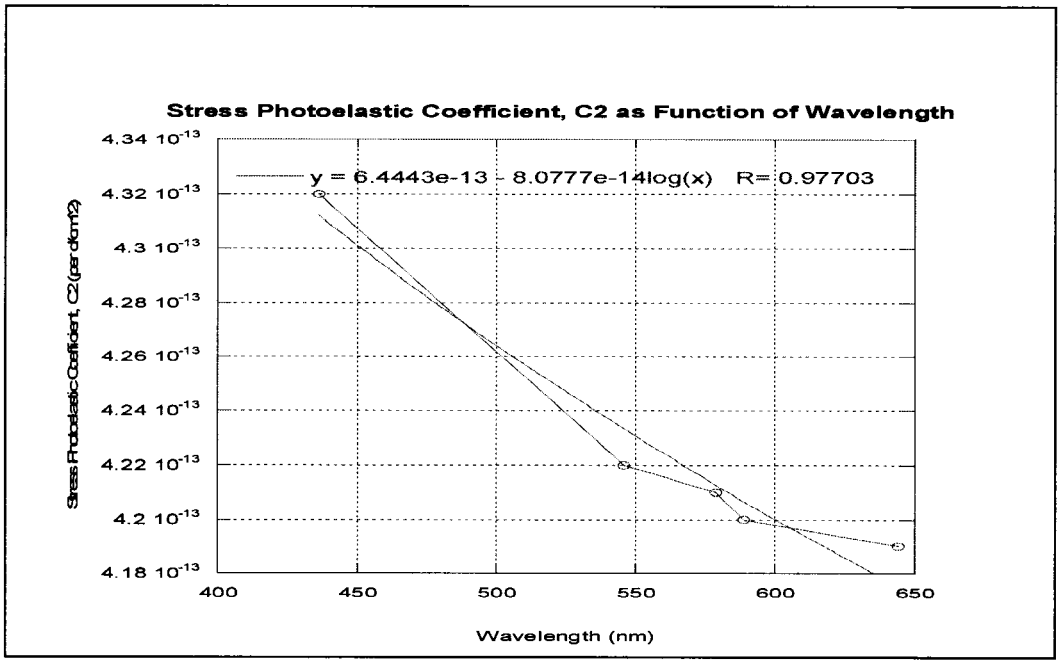

Figure 17. Fit data for stress optical coefficient C2 as function of wavelength.

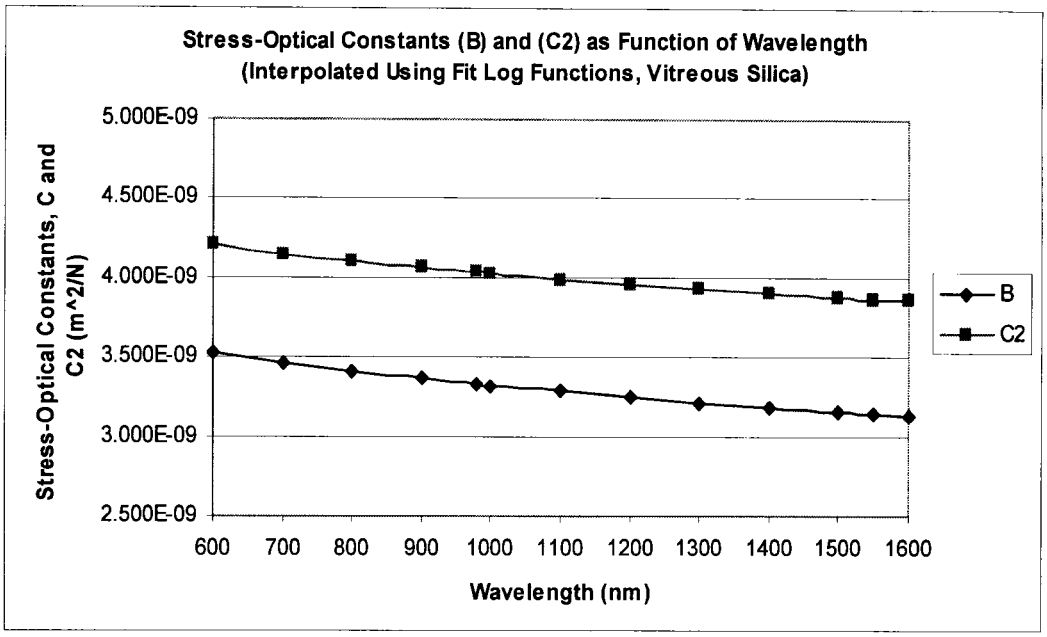

Figure 18. Interpolated functions for B and C2 as function of wavelength.

1.7 Bending stress in optical fibers

Stress distribution as a function of bend radius can be calculated using the equation for bending of beam [36]. The material is assumed to be elastic. The bending stress relates to the bend radius as:

$$\rho = -Ey / \sigma$$

where ρ is the bend radius, E is the Modulus of Elasticity, y is the radial location of stress, maximum at core radius, and σ is the axial stress in the x direction. Figure 19 shows the deformation segment of beam in bending. The assumption here is that the

bending of fiber would result in stress components that only the axial tension is significant. Thus, the transverse component is small and omitted.

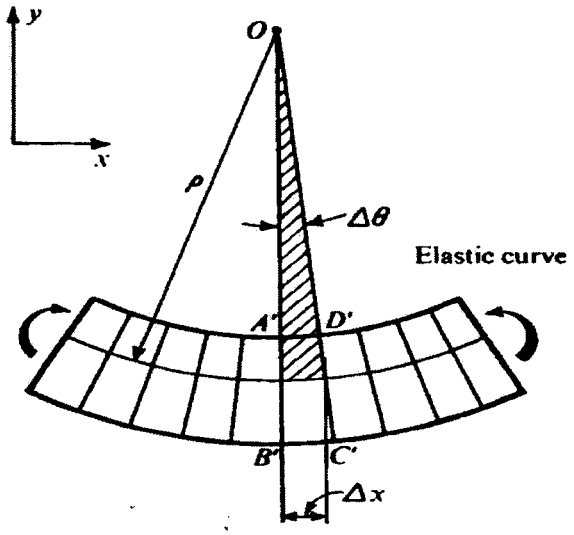

Figure 19. Deformation of a beam segment in bending [36].

The bending rupture of fiber is modeled using the tensile strength data by Griffith, which is complied by Morey [37], and interpolated for our fiber diameter of 125um. Here it is assumed that the core and cladding share the same material property of fused silica, and there is no residual stress at the boundary of the core and cladding, because the silica at the boundary is fused together between the core and the cladding forming a rigid interface condition. The resulting tensile strength for 125um fiber is about 288 MPa, which would result in fiber rupture at approximately 16mm bend radius. Griffith experimental data for tensile strength for glass fiber is shown in Table 3 for diameters from 0.0033mm to 1.0160mm.

Diameter (mm)	Tensile Strength (Kilobars)	Tensile Strength (MPa)
1.01600	1.715	171.5
0.10670	2.912	291.2
0.07060	3.498	349.8
0.05710	4.413	441.3
0.05080	5.480	548.0
0.04700	6.094	609.4
0.04440	5.688	568.8
0.03550	5.868	586.8
0.03350	6.850	685.0
0.02920	6.109	610.9
0.02410	8.053	805.3
0.01910	9.227	922.7
0.01780	11.295	1129.5
0.01520	12.720	1272.0
0.01420	10.600	1060.0
0.01270	13.410	1341.0
0.00970	15.980	1598.0
0.00660	22.830	2283.0
0.00418	34.300	3430.0
0.00330	33.830	3383.0

Table 3. Tensile strength for silica glass fiber of 0.0033 to 1.0160 mm diameter.

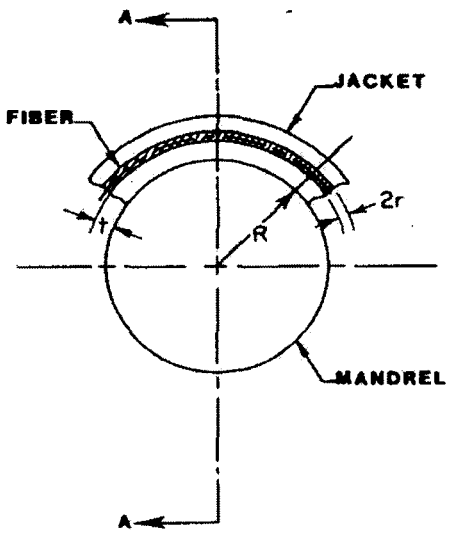

Figure 20. Geometry of a fiber bent over a mandrel [38].

To verify the result of stress distribution due to bending, a second method is used to compare the stress result due to fiber bending. This method is looking at the stress and strain relationships which have been developed with certain bending parameters. Figure 20 illustrates this schematic.

The strain relationship due to bending, ε, is shown for the mandrel method:

$$\epsilon = \frac{L - L_0}{L} = \frac{(R + t + 2r)\theta - (R + t + r)\theta}{(R + t + r)\theta} = \frac{r}{R + t + r} \qquad [37]$$

Here, R is the radius of the mandrel, r is the fiber radius, and t is the cladding thickness. Bending stress, σ, can be related to strain as follow:

$$\sigma = \varepsilon E = Er/(R+t+r)$$

For fused silica glass, Young's modulus of elasticity is about 7.4E10 N/m^2, which is assumed to be an average value and is used to calculate the bending stress on optical fiber. For a singlemode fiber with core diameter of 8 um and cladding diameter of 125 um, the bending stress calculation has been done to show the relationship of bending stress and bend radius. Figure 21 shows the bending stress using the beam method and the mandrel method. The two curves overlap each other, because the two methods reaffirm each other very well within or less than 0.4% error at 16mm bend radius and through out the bending radius range.

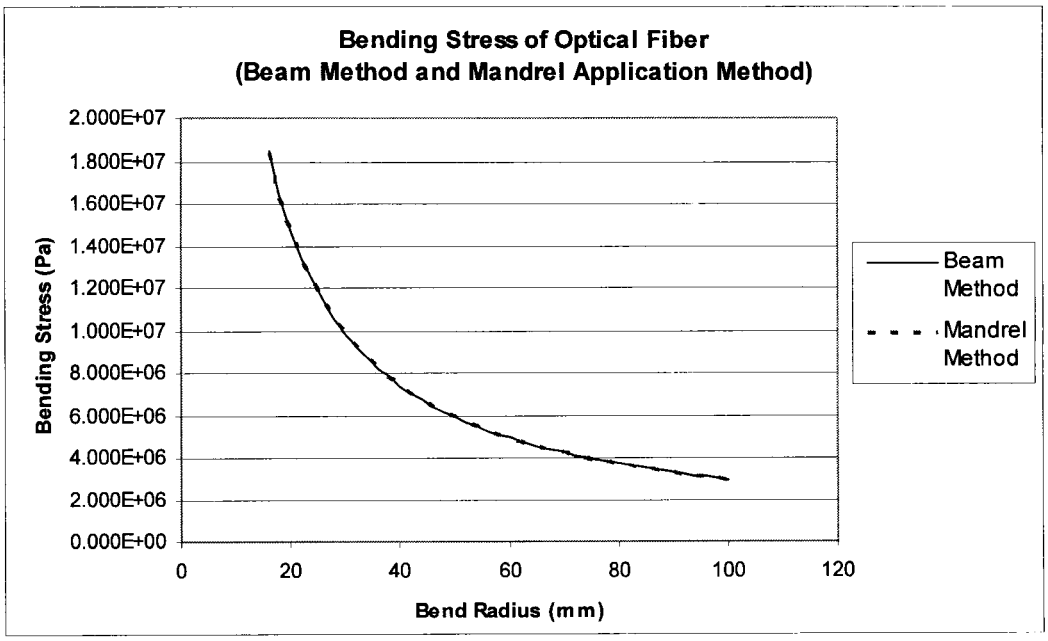

Figure 21. Bending stress of an optical fiber using the beam and mandrel methods.

1.8 Refractive index dependency on wavelength and temperature

Fused silica (SiO_2), also known as vitreous silica, has been widely used in the optical industry because of its favorable characteristic for light transmission. The relationship of its index of refraction and wavelength is determined by the dispersion equation by Malitson [39]. The dispersion equation is shown below:

$$n^2-1=\frac{0.6961663\lambda^2}{\lambda^2-(0.0684043)^2}+\frac{0.4079426\lambda^2}{\lambda^2-(0.1162414)^2}+\frac{0.8974794\lambda^2}{\lambda^2-(9.896161)^2}, \quad [38]$$

The values of index of refraction is calculated and shown in Table 4 and Figure 22 for different wavelengths. It is noticeable that index of refraction decreases with

higher wavelength. The dispersion equation is graphically processed for 12 specimens at 20°C. Index of refraction at 25°C (room temp) is corrected by the temperature function by Sosman [40].

λ @ 25C (nm)	Index @ 20C	Index @ 25C, corrected
600	1.45804	1.45810
700	1.45529	1.45536
800	1.45332	1.45338
900	1.45175	1.45182
980	1.45067	1.45074
1000	1.45042	1.45048
1100	1.44920	1.44927
1200	1.44805	1.44811
1300	1.44692	1.44698
1400	1.44578	1.44584
1500	1.44462	1.44468
1550	1.44402	1.44409
1600	1.44342	1.44348

Table 4. Index of refraction as function of wavelength for fused silica.

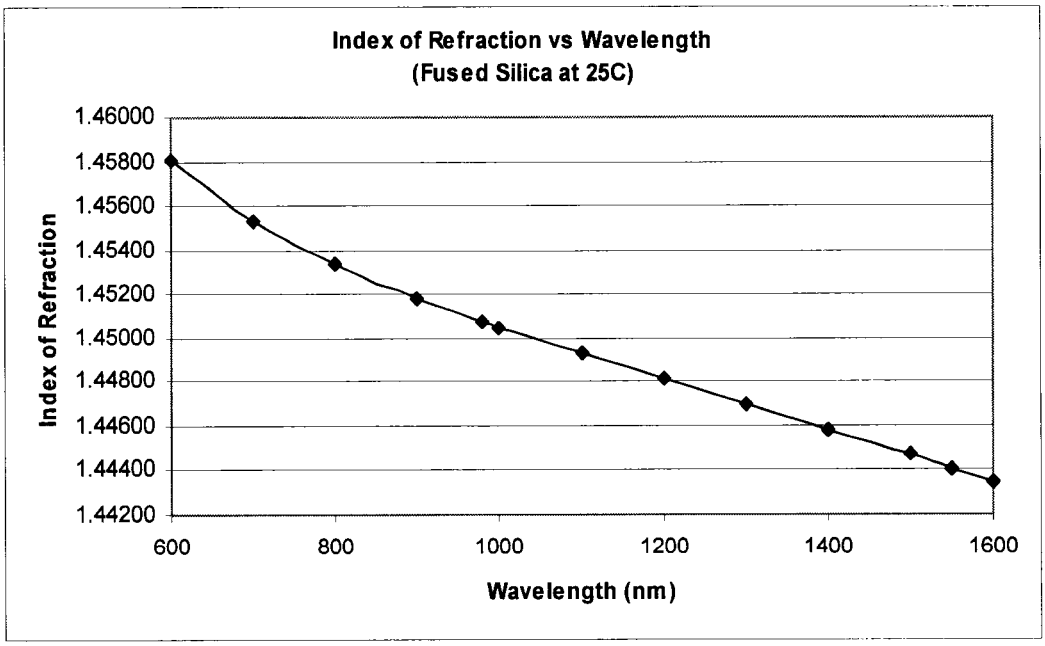

Figure 22. Index of refraction plot as a function of wavelength.

Sosman's work on the properties of silica combines together the correction of index of refraction from Rhine, the coefficient of thermal expansion data from Callendar, and the modulus data from Horton. Table 5 shows the temperature dependency of index of refraction and in a separate column shown on the right most is the interpolation for 600nm wavelength. The data was obtained by Rhine for the chosen wavelengths of 471.315um, 501.568um, 587.563um, and 667.815um because they are the stable and fixed wavelengths for helium blue, helium green, helium yellow, and helium red noble gases, respectively. Figure 23 shows the change of index of refraction with temperature and it holds much of the linear relationship with temperature from 25°C up to 1000°C. With reference to 25°C, the refractive index change at 1000°C is 0.01363. Figure 24 is plotted for some telecom wavelengths like 980nm, 1300nm, and 1550nm. Here the rate of change of refractive index with temperature is about the same for all three wavelengths. Figures 25 and 26 show the temperature functions of coefficient of thermal expansion and modulus of elasticity. Modulus of elasticity reaches a plateau of 74GPa at 800°C to 900°C, and drops off at higher temperatures. It is proportional to modulus of rigidity, in which the data is derived.

Temp (C)	λ = 471.315um (He blue)	λ = 501.568um (He green)	λ = 587.563um (He yellow)	λ = 667.815um (He red)	λ = 600 um
-160	1.4635	1.4617	1.4581	1.4559	**1.45776**
-64	1.4641	1.4624	1.4586	1.4563	**1.45824**
18	1.4649	1.4629	1.4592	1.4569	**1.45884**
25	**1.4650**	**1.4630**	**1.4593**	**1.4570**	**1.45892**
130	1.4660	1.4642	1.4604	1.4579	**1.46001**
235	1.4675	1.4654	1.4616	1.4591	**1.46121**
365	1.4692	1.4672	1.4633	1.4608	**1.46291**
475	1.4708	1.4689	1.4649	1.4625	**1.46453**
590	1.4722	1.4703	1.4663	1.4639	**1.46593**
1000	--	1.4772	1.4729	1.4706	**1.47254**

Table 5. Index of refraction as function of temperature for fused silica [40].

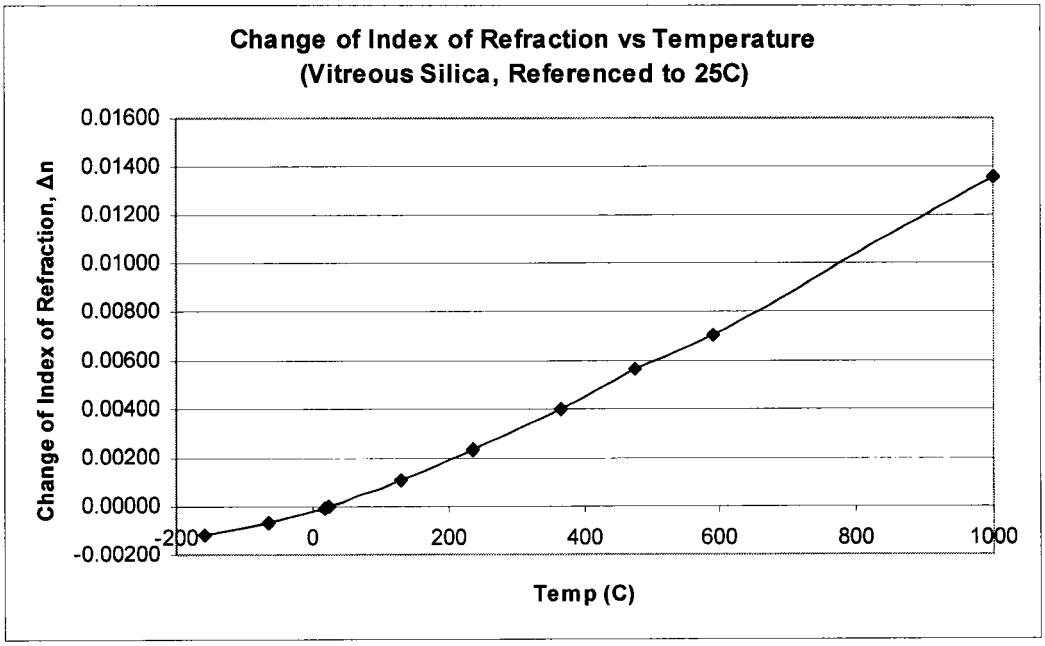

Figure 23. Change of refractive index as function of temperature.

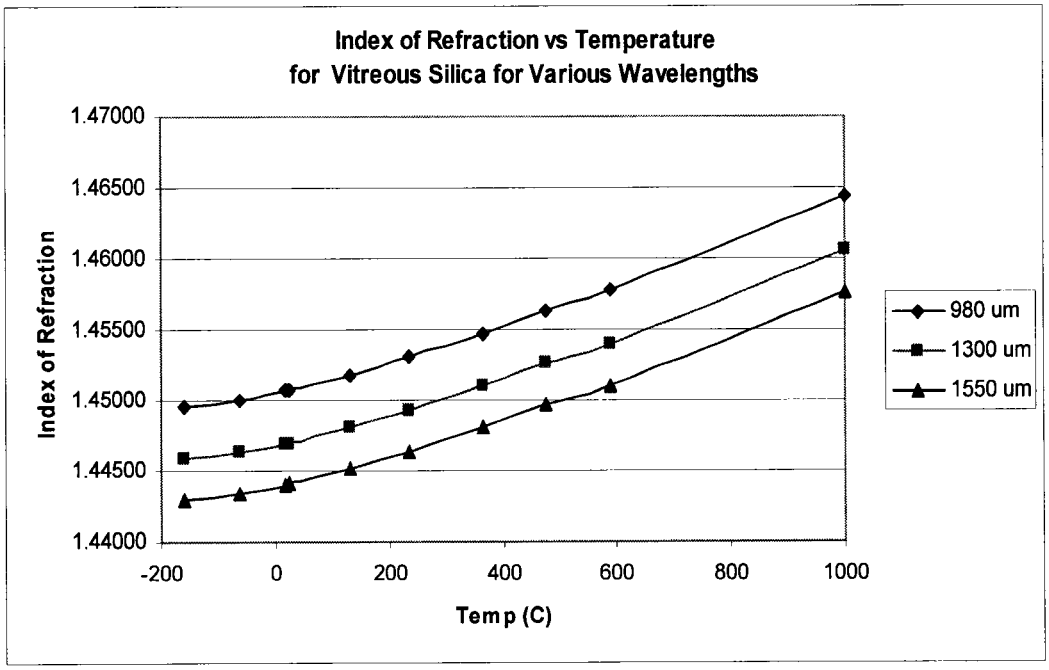

Figure 24. Index of refraction as function of temperature for chosen wavelengths.

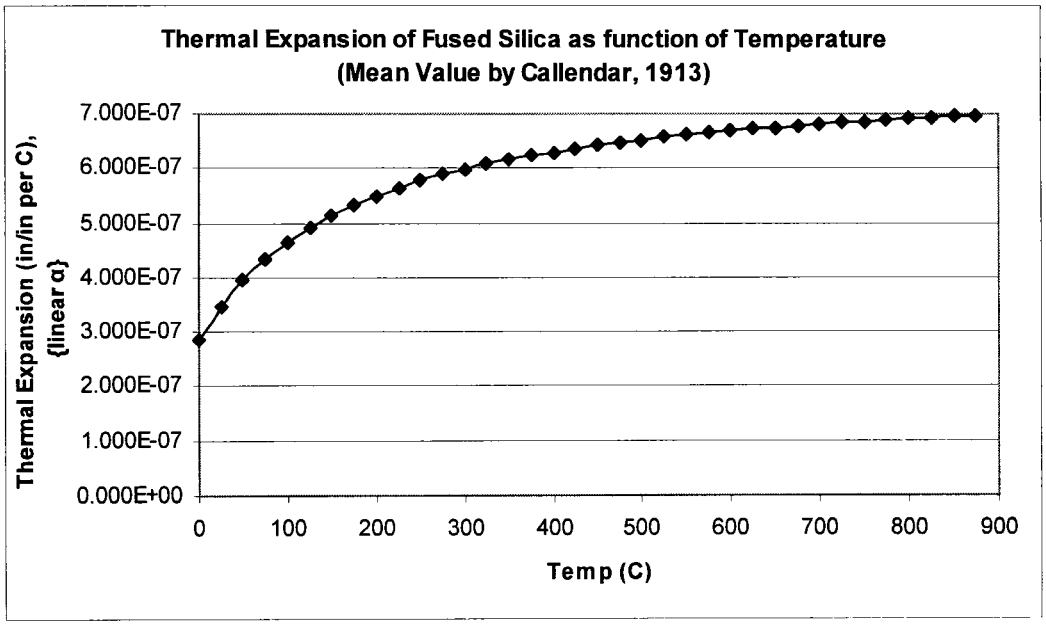

Figure 25. Thermal expansion coefficient as function of temperature for fused silica.

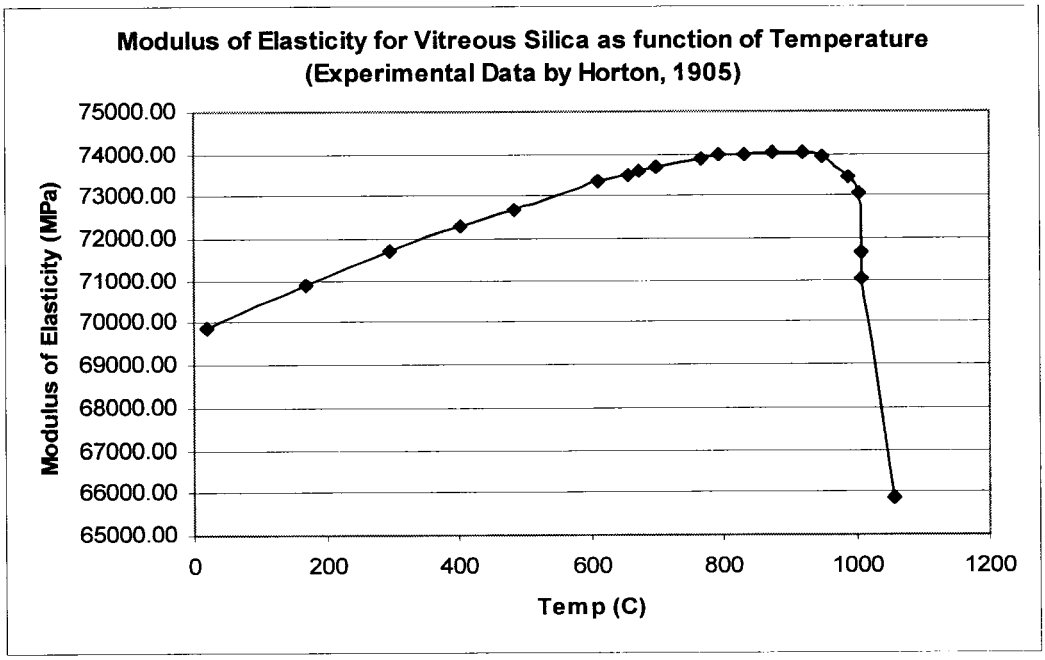

Figure 26. Modulus of elasticity as function of temperature for fused (vitreous) silica.

1.9 Thermal stress at boundary of fiber core and cladding

It is important to study the thermal stress occurring at the boundary of the core and cladding, because the thermal stress would introduce certain change in index of refraction as the result of the additional axial stress exerted on the core. This only happens when the core and cladding are of two different materials and thus resulting in a situation of coefficient of thermal expansion mismatch. If the core and cladding of the fiber is made of fused silica, the thermal stress due to CTE mismatch is zero. However, it is a common practice to strengthen the glass by introducing surface compression, since glass breaks from the surface in tension. The thermal stress is observed during the manufacturing of fiber, with the cladding sets at a higher temperature than the core and then both as a fiber cool to room temperature. The core is assumed to be made of fused silica glass, and the cladding is made of borosilicate glass. The borosilicate glass value of the thermal coefficient of expansion is taken as 3.2E-6 (in/in per °C) [41]. It is also assumed that the stress level resulting from heating the fiber, from room temperature to an elevated temperature, would experience the same level as that when being cooled from manufacturing with a reverse range.

The axial component of thermal stress (Pz2) between core and cladding resulting from being cooled to room temperature is derived by Scherer and Cooper [42]:

$$Pz2 = [(\alpha 2 - \alpha 1)(Ts1 - Tr)E2 / (1-\nu 2)] * (a/b)^2$$

where $\alpha 1$ and $\alpha 2$ are coefficients of thermal expansion for the core and the cladding,

respectively, T_{s1} is the setting temperature of the core and T_r is room temperature, E_2 is modulus of elasticity of the cladding, ν is Poisson ratio, and a and b are the radii of the core and the cladding, respectively. It is pointed out by Scholes that the setting temperature for fused silica (T_{s1}) is about 870°C [43]. Table 6 and Figure 27 show the temperature characteristic of fused silica and borosilicate glass for temperatures up to 870°C. The data for borosilicate are obtained by assuming the value of coefficient of thermal expansion at 25°C to be 3.2E-6 (in/in per °C) [see 41], and by assuming that its thermal property would follow the characteristic of fused silica. It is an acceptable assumption because fused silica has SiO_2 content of 96.3% and borosilicate glass has SiO_2 content of 80.5%; both are close in silica content and are commercially available, and the coefficient of thermal expansion relative change above 250°C is small.

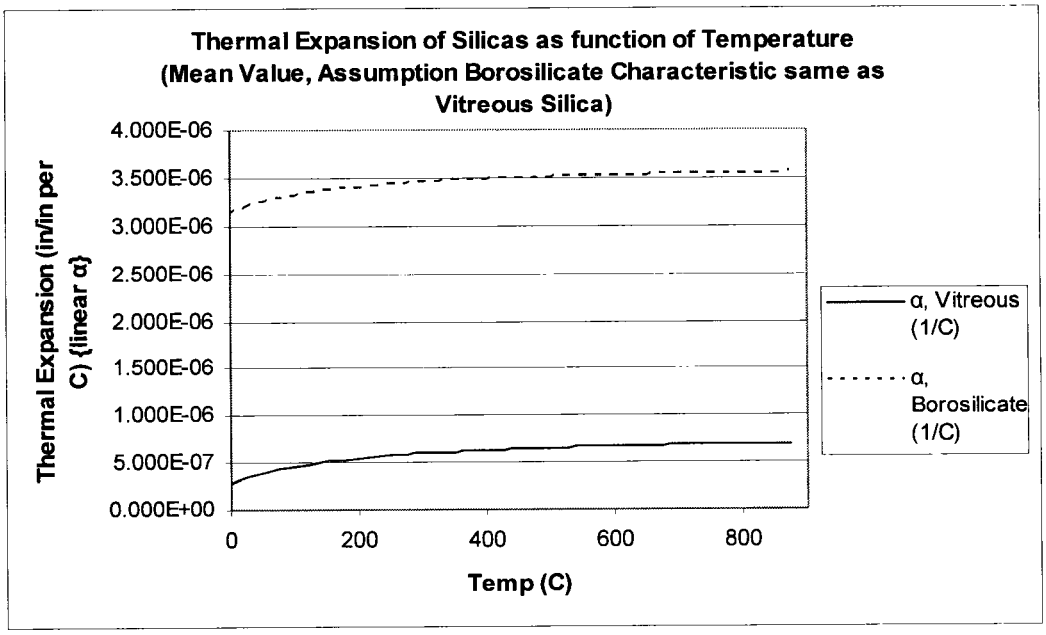

Figure 27. Thermal expansion coefficients of fused silica and borosilicate glass.

Temp ©	α, Vitreous (1/C)	α-Slope ref at 25C	α, Borosilicate (1/C)
0	2.857E-07	-6.179E-08	3.138E-06
25	**3.475E-07**	**0.000E+00**	**3.200E-06**
50	3.956E-07	4.806E-08	3.248E-06
75	4.340E-07	8.650E-08	3.287E-06
100	4.655E-07	1.180E-07	3.318E-06
125	4.917E-07	1.442E-07	3.344E-06
150	5.138E-07	1.663E-07	3.366E-06
175	5.329E-07	1.854E-07	3.385E-06
200	5.493E-07	2.018E-07	3.402E-06
225	5.638E-07	2.163E-07	3.416E-06
250	5.765E-07	2.290E-07	3.429E-06
275	5.878E-07	2.403E-07	3.440E-06
300	5.979E-07	2.504E-07	3.450E-06
325	6.070E-07	2.595E-07	3.460E-06
350	6.152E-07	2.677E-07	3.468E-06
375	6.227E-07	2.752E-07	3.475E-06
400	6.296E-07	2.821E-07	3.482E-06
425	6.358E-07	2.883E-07	3.488E-06
450	6.416E-07	2.941E-07	3.494E-06
475	6.469E-07	2.994E-07	3.499E-06
500	6.519E-07	3.044E-07	3.504E-06
525	6.564E-07	3.089E-07	3.509E-06
550	6.607E-07	3.132E-07	3.513E-06
575	6.647E-07	3.172E-07	3.517E-06
600	6.684E-07	3.209E-07	3.521E-06
625	6.719E-07	3.244E-07	3.524E-06
650	6.752E-07	3.277E-07	3.528E-06
675	6.782E-07	3.307E-07	3.531E-06
700	6.811E-07	3.336E-07	3.534E-06
725	6.839E-07	3.364E-07	3.536E-06
750	6.865E-07	3.390E-07	3.539E-06
775	6.889E-07	3.414E-07	3.541E-06
800	6.913E-07	3.438E-07	3.544E-06
825	6.935E-07	3.460E-07	3.546E-06
850	6.956E-07	3.481E-07	3.548E-06
875	6.976E-07	3.501E-07	3.550E-06

Table 6. Dilatation of fused silica and borosilicate glass as function of temperature.

CHAPTER 2

Research Objectives and Hypothesis

The important optical characteristics of singlemode fiber that determine the signal quality, data transfer rate, and studied in this research are attenuation, dispersion, and birefringence. The singlemode fiber construction is very small in diameter and made of fused silica glass, and its performance is very sensitive to environmental factors such as stress due to external disturbances, and environmental and application temperatures. Fiber Bragg Grating is a new technology in sensing application and is commonly used in areas where ordinary sensors cannot. The grating is inscribed into the glass core of the fiber, where its sensitivity to strain, resulting from external stress, and temperature would result in its light wavelength shift.

The objectives of this research are to study the effect of stress due to bending and the effect of temperature on fiber performance characteristics such as attenuation, dispersion, and birefringence, and also to study the influence of these bending and temperature effects on the change of property and performance of Fiber Bragg Grating. The hypothesis is that the change in optical performance of singlemode fiber is resulting from the change of index of refraction of silica glass due to external stress and temperature effects and the change or shift in Bragg grating wavelength is resulting from grating sensitivity to external strain and temperature effects. Since the grating is inscribed onto the core of the fiber, the effects are considered to be the same levels as those that the singlemode fiber would experience.

CHAPTER 3

Modeling

3.1 Finite element analysis model of fiber bending

The bending of singlemode fiber is modeled in finite element analysis using the software code ABAQUS version 6.4-1 [44]. The primary objective of the finite element analysis is to make comparative study of stress distribution levels on the core of the optical singlemode fiber as a function of bend radius to that of the analytical beam model. The stress distribution is present as the fiber core is bent to form about the mandrel with different radii for different cases. The dimensional units for all cases of study in this report are in Newton unit for force and millimeters unit for length. The singlemode fiber core is modeled as a thin cylinder with diameter of 8um, of the material of fused silica with modulus of elasticity of 74,000 N/mm^2 (74GPa) and Poisson ratio of 0.164. The mandrel is modeled as a wedge, with 0.100 mm thick, to represent a rigid mold, where deformation is negligible. The value of the thickness of the mandrel is chosen to minimize the number of elements in the mesh model, and it is of enough thickness to accommodate the 8um diameter fiber core. The property for the mandrel is given with modulus of elasticity of 7.4E10 N/mm^2, assigned roughly about a million times stiffer than that of fused silica, and Poisson ratio similar to fused silica of 0.164. The mandrel or bend radii of study are 16mm, 24mm, 32mm, and 40mm. To reduce the model size and computational time, the fiber core length is modeled with only 5mm in length. The model of the fiber core is meshed with tetrahedral elements with 8 elements in the fiber core cross-section, and meshed through out the 5 mm length of the fiber with the total of

11,992 elements. The meshing on the mandrel is done with a much course element grid, since the interest is in the core fiber. Figure 28 shows the meshing of the fiber core in wire frame mode with tetrahedral elements.

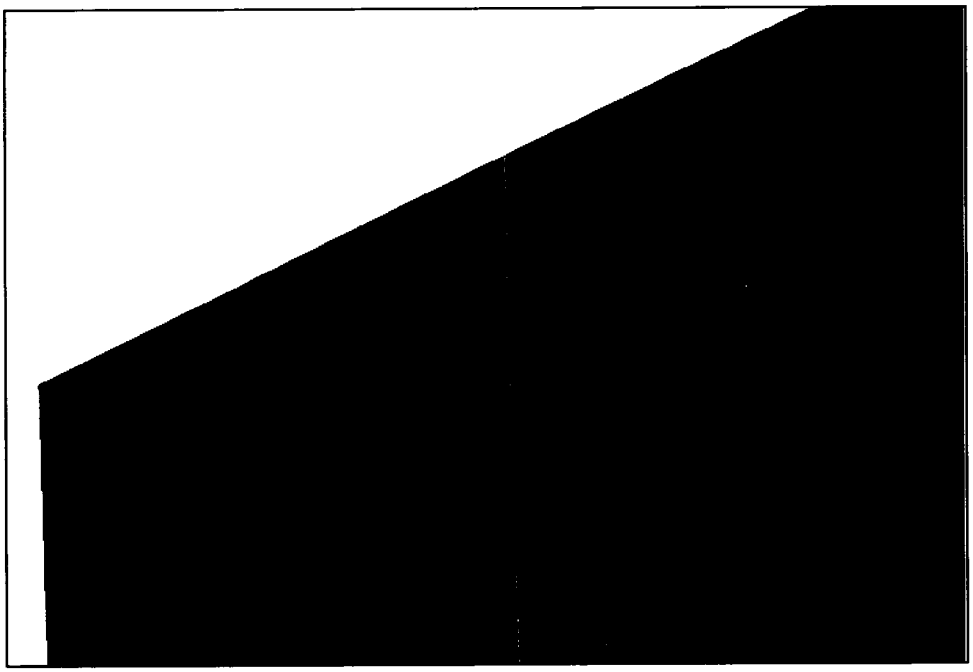

Figure 28. The tetrahedral meshing model of fiber core.

The boundary conditions are set to simulate the condition of fiber bending when the fiber is wrapped on the fiber spool. The label for the axis is shown with direction 1 for X, direction for Y, and direction 3 for Z. To form a curvature around the mandrel, one end of the fiber core is fixed in X direction, and the nodes along the fiber top are fixed in Z direction. Rotations of the fiber are not constrained. The fiber core is assigned as the "slave" surface, where it is allowed to conform to the "master" surface, of which is assigned to the mandrel curve surface. The fiber is assigned a body force of 0.75 N in the

downward Y direction. This value is selected to allow the fiber core to fully forming the arch to the mandrel. In the model, the mandrel is fixed in both vertical and horizontal surfaces. Figure 29 shows the details with yellow arrows as the body force and the orange triangles as the boundary conditions.

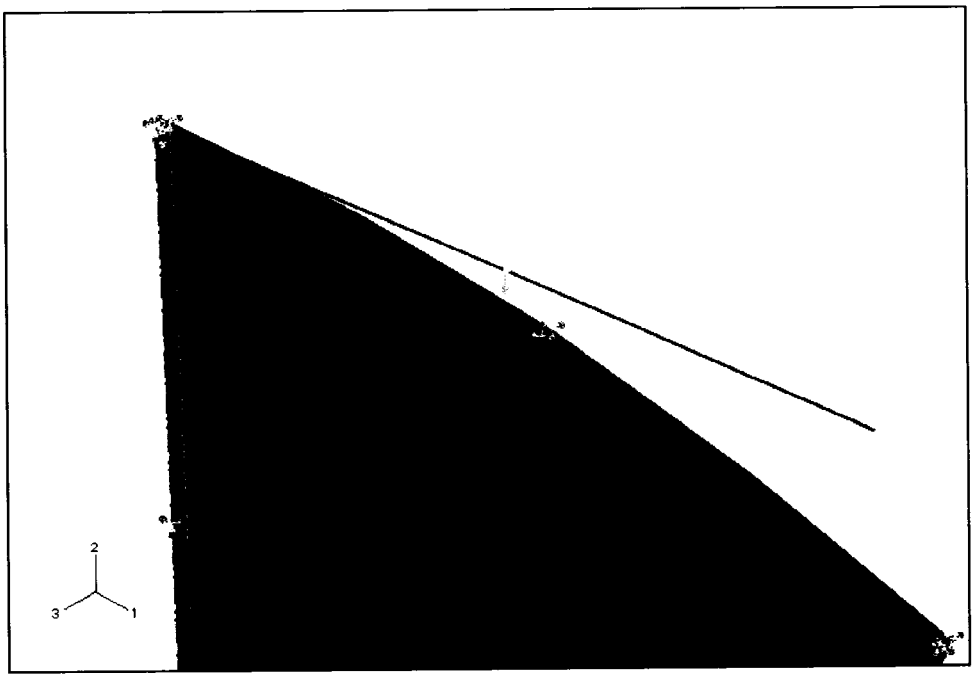

Figure 29. Boundary conditions of optical fiber core and mandrel.

3.2 Principal stress distribution results of different bend radii

Stress distributions due to bending of the fiber core are shown in Figures 30, 34, 35, and 36 for bend radii of 16mm, 24mm, 32mm, and 40mm, respectively. The significance of 16mm bend radius is that it is the critical bend radius of 8um core diameter singlemode fiber before fracture, and 40mm bend radius is the condition where the interested phenomenon of attenuation level is negligible. The bend radii of 24mm

and 32mm are data points that fit in between the extremes. The finite element analysis results give approximate maximum principal stress of 21.12 N/mm^2 with 16mm bend radius, 14.24 N/mm^2 with 24mm bend radius, 10.55 N/mm^2 with 32mm bend radius, and 7.41 N/mm^2 with 40mm bend radius. Note that these stress values are given by the color coded legend with the estimated highest values of their respective color levels. These levels of maximum principal stress are compared to those of analytical beam model and are matched in a reasonable sense, with the largest error in value of 15.49% at 24mm bend radius condition. The overall higher stress conditions result in the range about 14% to 15.5% of error. The complete summary is shown in Table 7. The sources of error in the results of the finite element analysis solution are due to the accuracy in element type and element size used in the model. The tetrahedral elements used in the model have a lesser degree of accuracy in comparison to that of the higher order types like hexagonal elements. To use the hexagonal elements in the model, it enormously increases the model size due to a requirement of a much finer partitions and elements in meshing the model, thus increasing the computational time required. The finer element size, however, gives better accuracy results.

Fiber Bend Radius (mm)	Analytical Beam Solution (N/mm²)	Abaqus FEA Solution (N/mm²)	% Error
16	18.50	21.120	14.16
24	12.33	14.240	15.49
32	9.25	10.550	14.05
40	7.40	7.419	0.26

Table 7. Maximum principal stress of fiber bending for different bend radii.

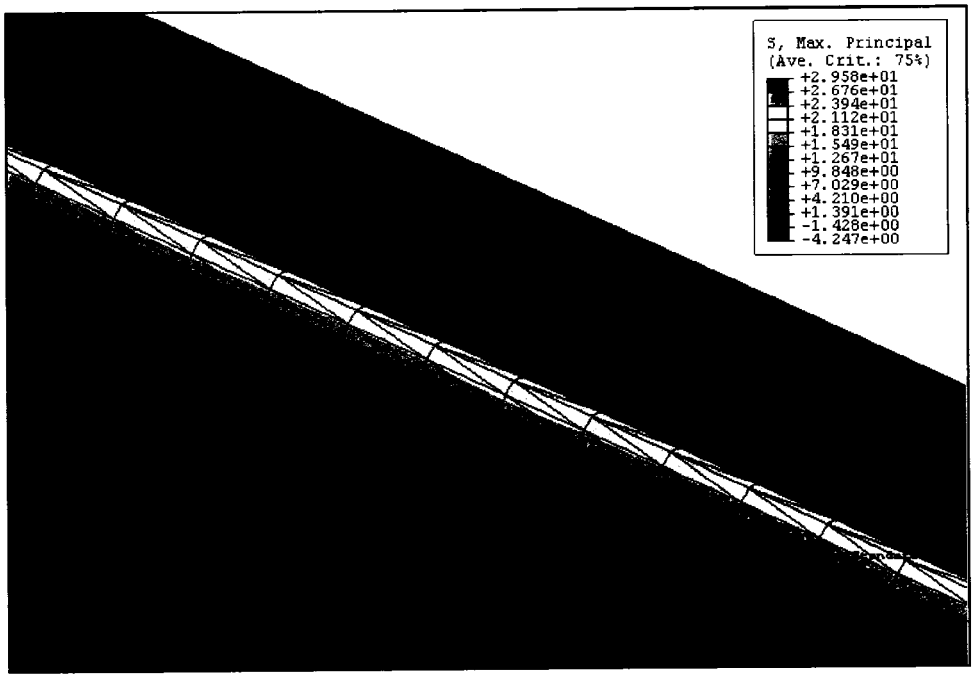

Figure 30. Maximum principal stress of fiber core with 16mm bend radius.

It is observed that the stress distribution is peak at the top regions of the fiber core, and this is also confirmed with that of the beam theory that maximum tensile stress occurs at the top due to bending. Figure 31, the fiber fixed boundary condition end, shows that there is a distribution of stress across the upper-half of the fiber core section in the Y direction of about 3 N/mm^2. In the calculation of optical properties of singlemode fiber, the stress field value is taken as the peak analytical value at fiber core top and assumed to be uniform across the fiber core. An interesting result to notice also is the value of Von Mises stress, which is the square root of the sum of the squares of all stress components, is about 26.64 N/mm^2 with 16 mm bend radius. This is about 20% higher than that of the maximum principal stress at the same bending condition of 16mm radius. Figures 32 and 33 show the Von Mises stress on the fiber core in the elastic region.

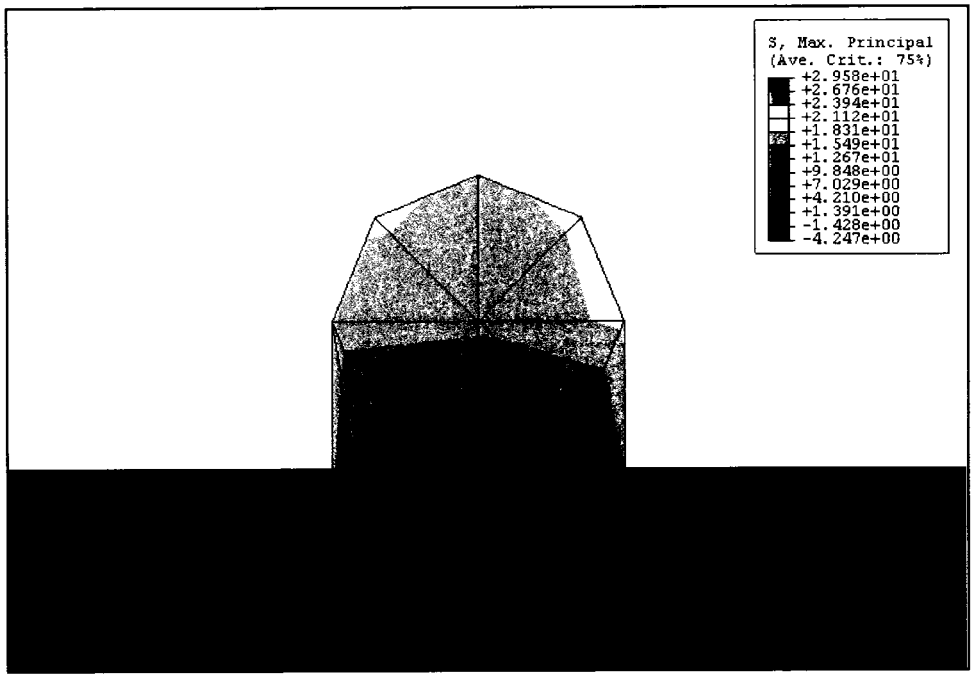

Figure 31. Maximum principal stress profile at fiber end for 16mm bend radius.

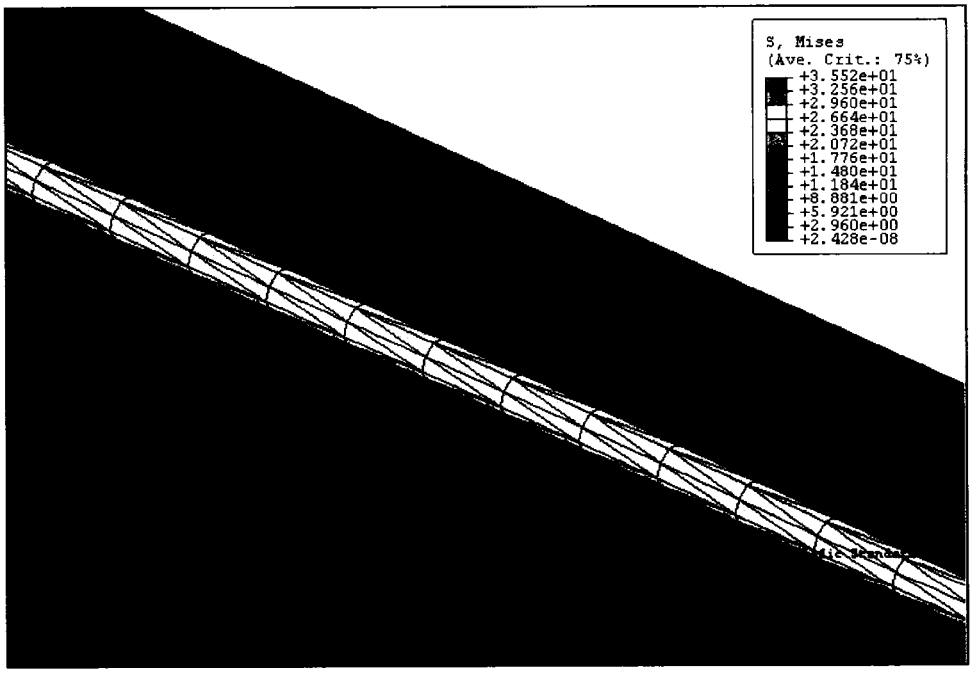

Figure 32. Von Mises stress of fiber core with 16mm bend radius.

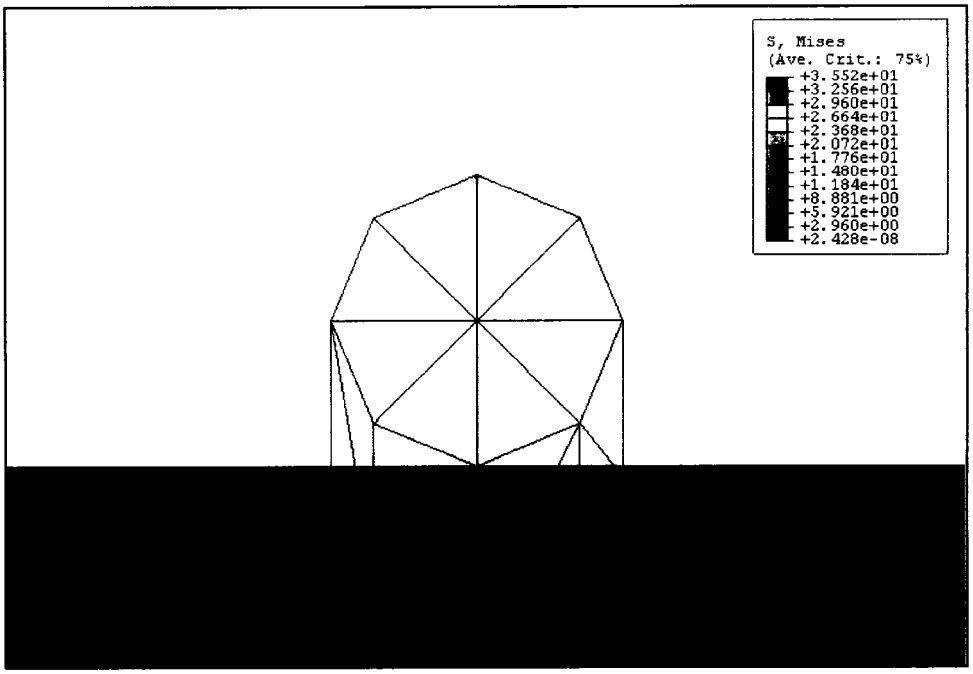

Figure 33. Von Mises stress profile at fiber end for 16mm bend radius.

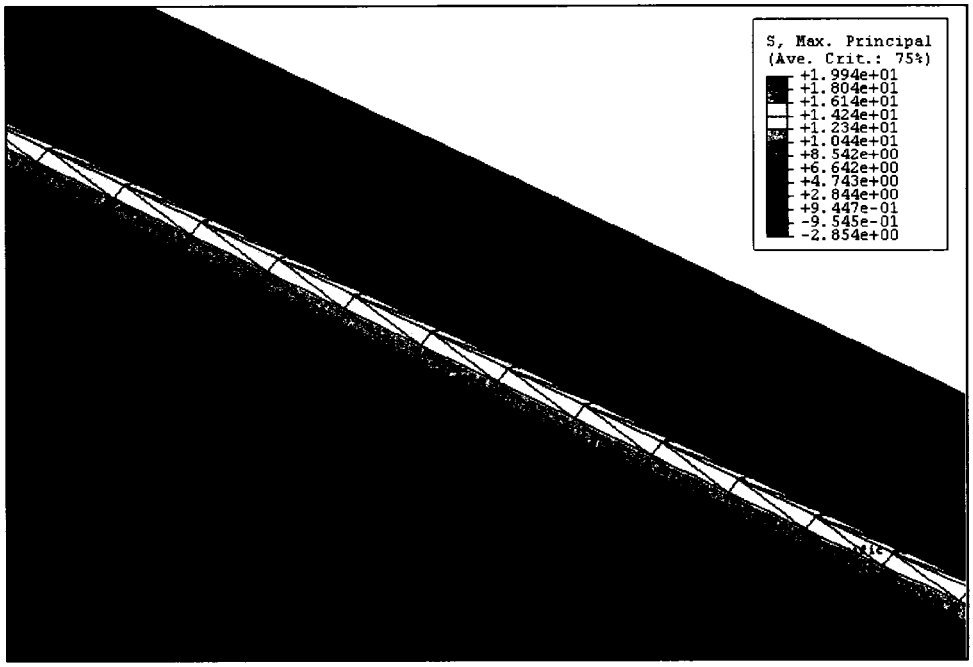

Figure 34. Maximum principal stress of fiber core with 24mm bend radius.

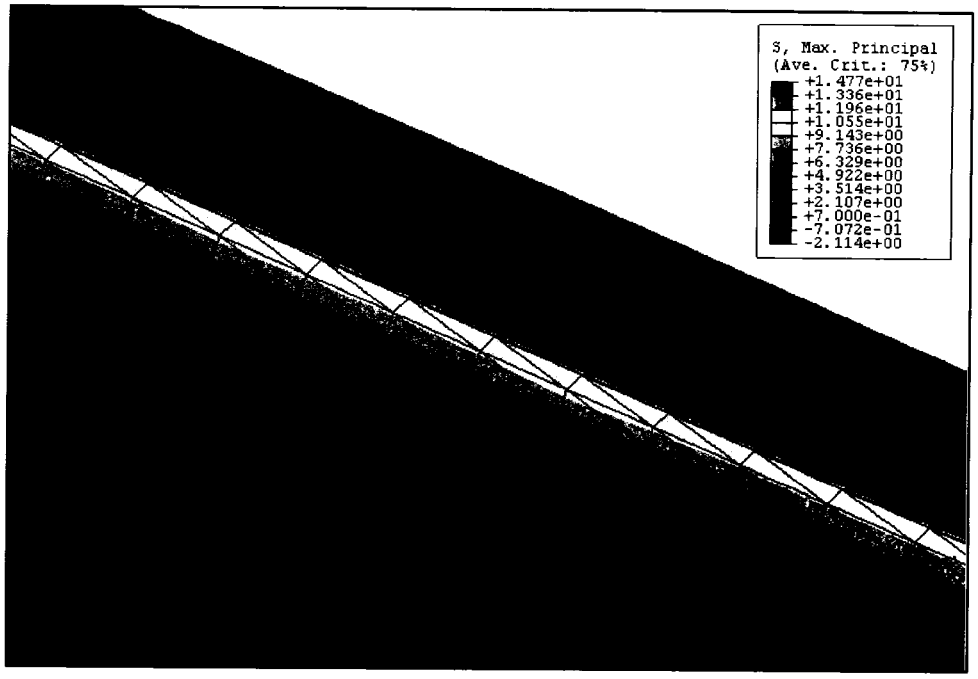

Figure 35. Maximum principal stress of fiber core with 32mm bend radius.

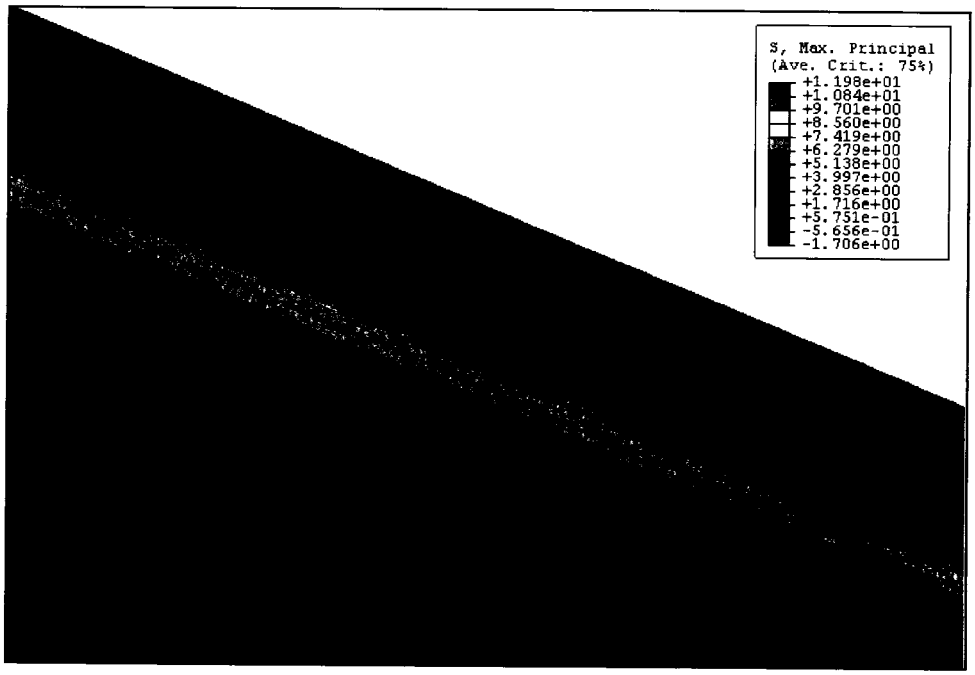

Figure 36. Maximum principal stress of fiber core with 40mm bend radius.

CHAPTER 4

Results and Discussion

4.1 Change of index of refraction due to bending stress

The change of index of refraction is calculated for the singlemode fiber with core diameter of 8um and cladding diameter of 125um. The stress calculation of the result from fiber bending as a function of bend radius is discussed in Section 1.7, and the photoelastic relationship between stress and index of refraction is discussed in Section 1.6. The result of index of refraction change with bend radius for fused silica is shown in Figure 37, for three wavelengths of 980nm, 1300nm, and 1550nm. It is observed that the change of refractive index increases linearly from unbent condition (bend radius at infinity) to approximately 200mm bend radius, then exponentially from 200mm to 16mm bend radius. At bend radius of 1000mm, the attenuation is approximately zero and it increases to about 0.06 at 16mm, the minimum allowable bend radius. The curves for the three wavelengths are almost overlapping with the plot scale to capture the magnitudes of attenuation for bend radius of 16mm to 1000mm. Figure 38 shows the close up detail of the region of bend radius of 16mm to 40mm. Here, the rate of change of refractive index is higher at lower wavelengths because it has a higher value of the photoelastic constant B, where B is a function of wavelength. At the 16mm bend radius condition, the change of index of refraction for 980nm, 1300nm, and 1550nm wavelengths are 0.62, 0.60, and 0.58, respectively.

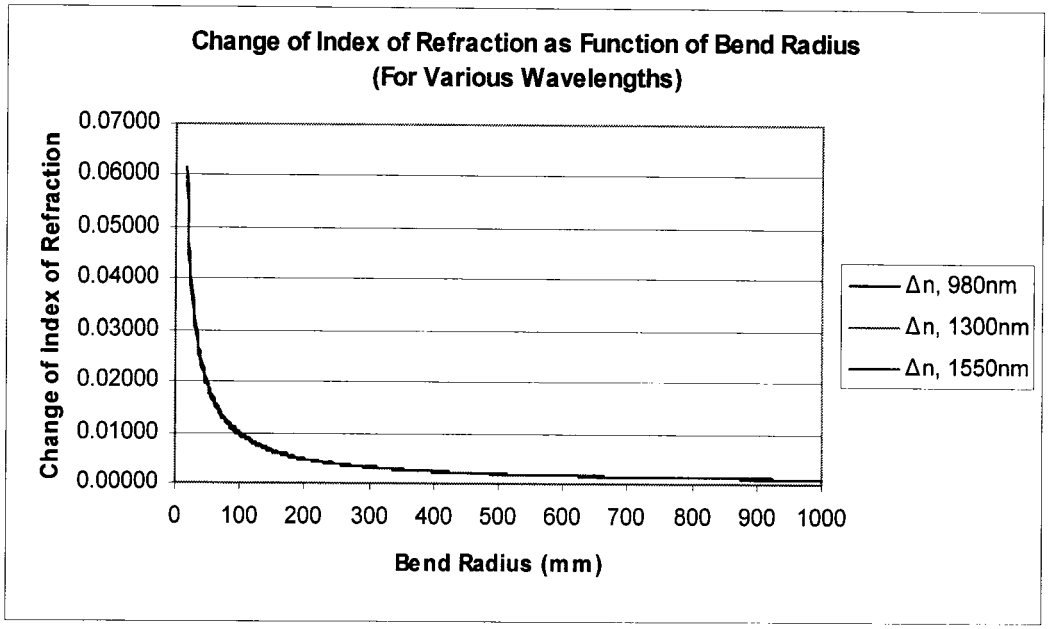

Figure 37. The change of refractive index as function of fiber bend radius.

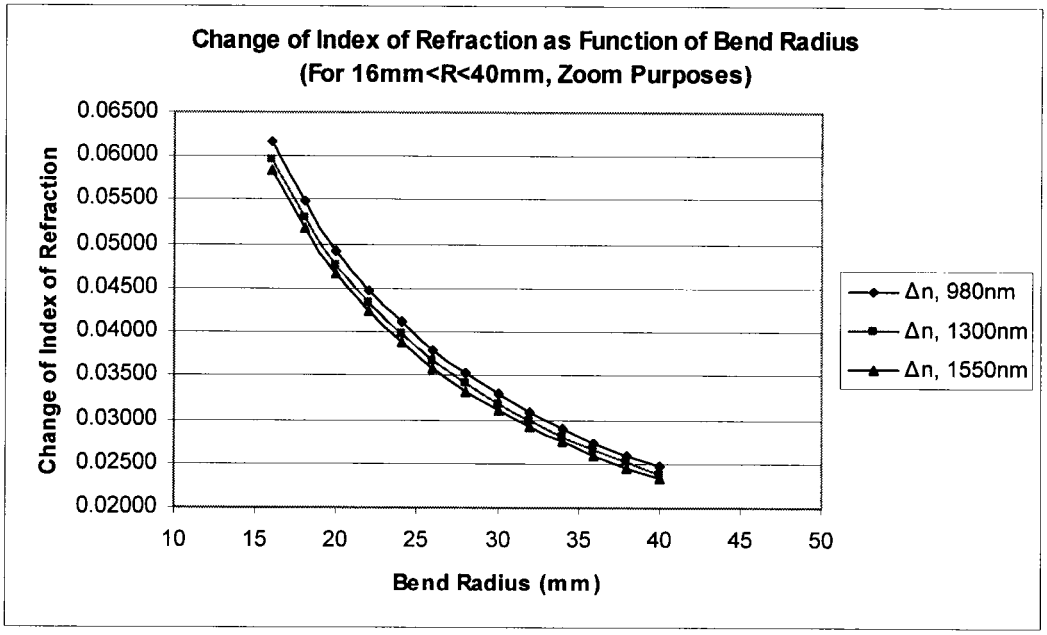

Figure 38. The change of refractive index as function of fiber bend radius, from 16mm to 40mm.

4.2 Attenuation change with bending and temperature

Attenuation (2α) relationship is calculated for the singlemode fiber with core diameter of 8um and cladding diameter of 125um for three particular telecom wavelengths of 980nm, 1300nm, and 1550nm. The material of the fiber, for both the core and the cladding, is fused silica, also known as vitreous silica, unless otherwise noted. The index of refraction for fused silica is wavelength dependent and is discussed in Section 1.8. Some values of index of refraction for wavelengths of 980, 1300, and 1550 are 1.45074, 1.44698, and 1.44409, respectively. The difference between core and cladding index of refraction for light propagation is assumed to be 0.2 %.

Baseline models of the attenuation equation are calculated for wavelengths of 980nm, 1300nm, and 1550nm as a function of bend radius. They are only computed to show the dependency relationship of bend radius, and these models do not include the additional change of index of refraction resulting from strain due to bending effect. They are shown in Figures 39, 40, and 41. At wavelength 980nm, attenuation shows the highest value of 0.44 dB/km at the minimum allowable bend radius of 16mm. This value is small compared to those at same bending condition for 1300nm and 1550nm of 31.89 dB/km and 2993.85 dB/km! The attenuation then decreases exponentially as bend radius increases, and it becomes negligible at bend radius of about 40mm. In actual applications, attenuation loss of greater than a few dB/km is considered not acceptable, and geometries of core and cladding have to be changed to obtain a lower acceptable level. The other parameter that can be considered is the difference in index of core and cladding, which assumed in this study of 0.2%, but is not considered in the scope of this

research. It is observed, however, that attenuation is higher at higher wavelengths than lower wavelengths according to the attenuation (2α) equation.

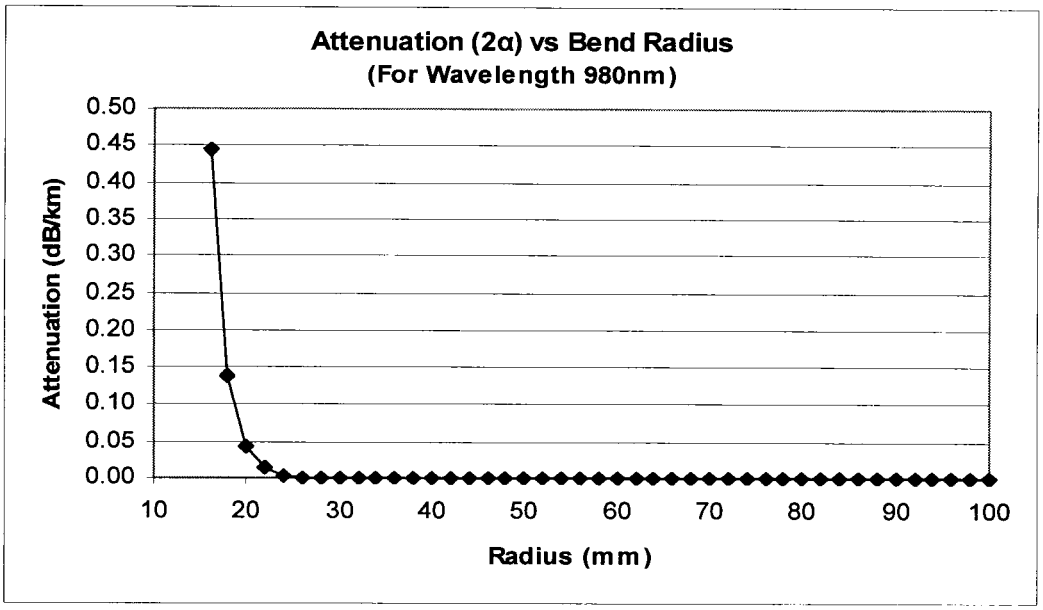

Figure 39. Attenuation of singlemode fiber at 980nm.

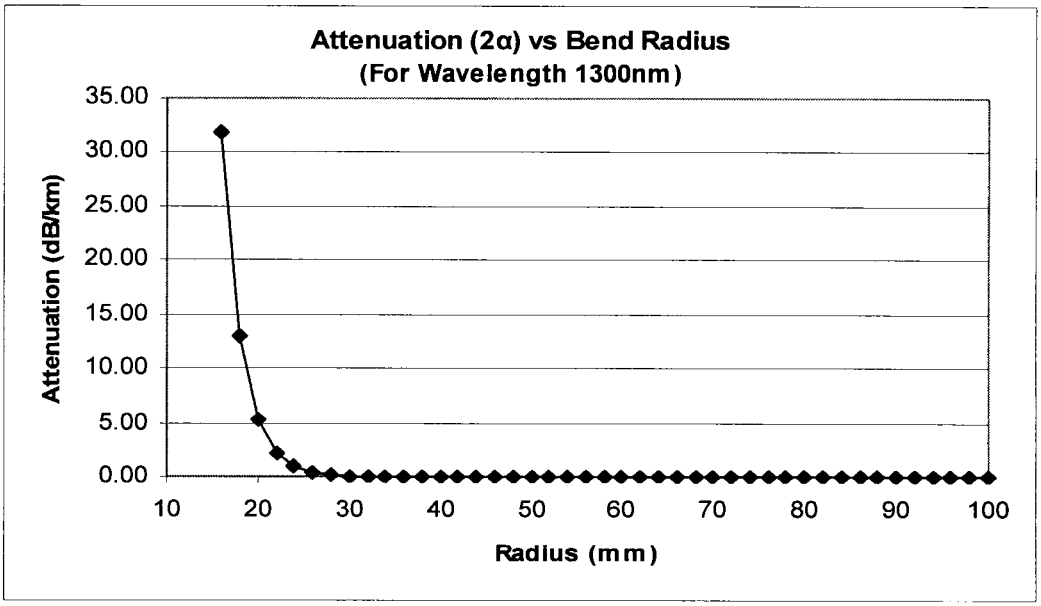

Figure 40. Attenuation of singlemode fiber at 1300nm.

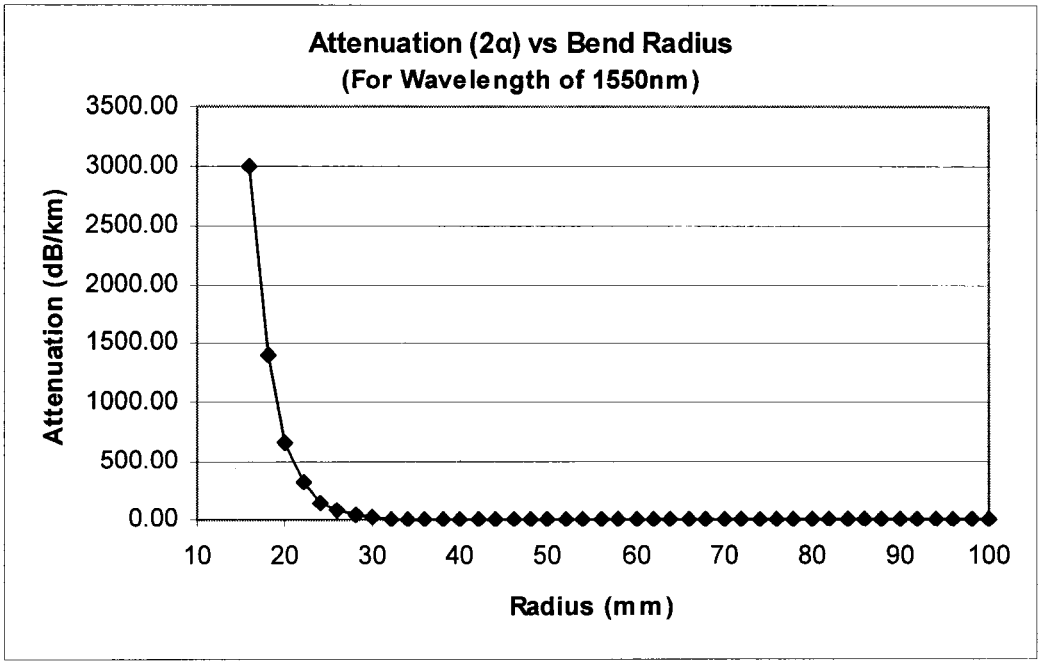

Figure 41. Attenuation of singlemode fiber at 1550nm.

Attenuation is being investigated for changing of the core geometry from the original of 8um in diameter to larger core diameters. Figures 42, 43, and 44 show the attenuations for core diameters of 9um, 10um, and 12um, respectively, for 980nm wavelength. The attenuation in the 9um geometry decreases from the 0.44 dB/km of 8um core diameter to 0.23 dB/km. Likewise, for 10um and 12um core geometries, the attenuations decrease to 0.14 dB/km and 0.06 dB/km, respectively.

For wavelength of 1300nm, Figures 45, 46, and 47, show the attenuation level for core geometries of 9um, 10um, and 12um, respectively. The attenuation levels decrease to 10.80 dB/km, 5.11 dB/km, and 1.79 dB/km, for cores of 9um, 10um, and 12um, respectively, from 31.89 dB/km for the 8um core geometry.

For a wavelength of 1550nm, Figures 48, 49, and 50, show the level of

attenuation for core geometry of 9um, 10um, and 12um, respectively. These conditions result in attenuation of 182.76 dB/km, 54.65 dB/km, and 13.46 dB/km. These values are significantly lower than that of 2993.85 dB/km for the 8um core diameter, at 16mm bend radius, but they still not acceptable on level of standard of today's telecom network. Core geometry has to be accommodated further to achieve acceptable attenuation level or it is required to defined a minimum bend application radius of some value larger than 16mm, for it to work at this wavelength.

The observed trend for attenuation and core geometry is of such that when the core diameter increases, the attenuation level decreases. This perhaps can be explained by having a larger waveguide in form of a larger core diameter, and therefore it reduces light scattering for the same distance of light propagation, thus lowering the overall attenuation level.

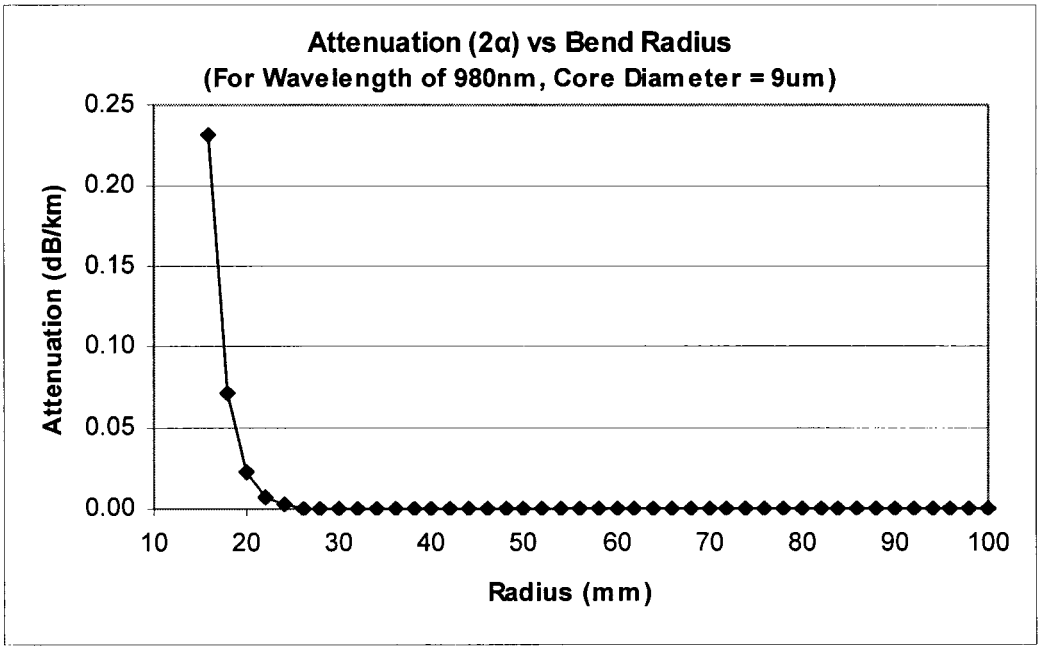

Figure 42. Attenuation for singlemode fiber with core diameter of 9um at 980nm.

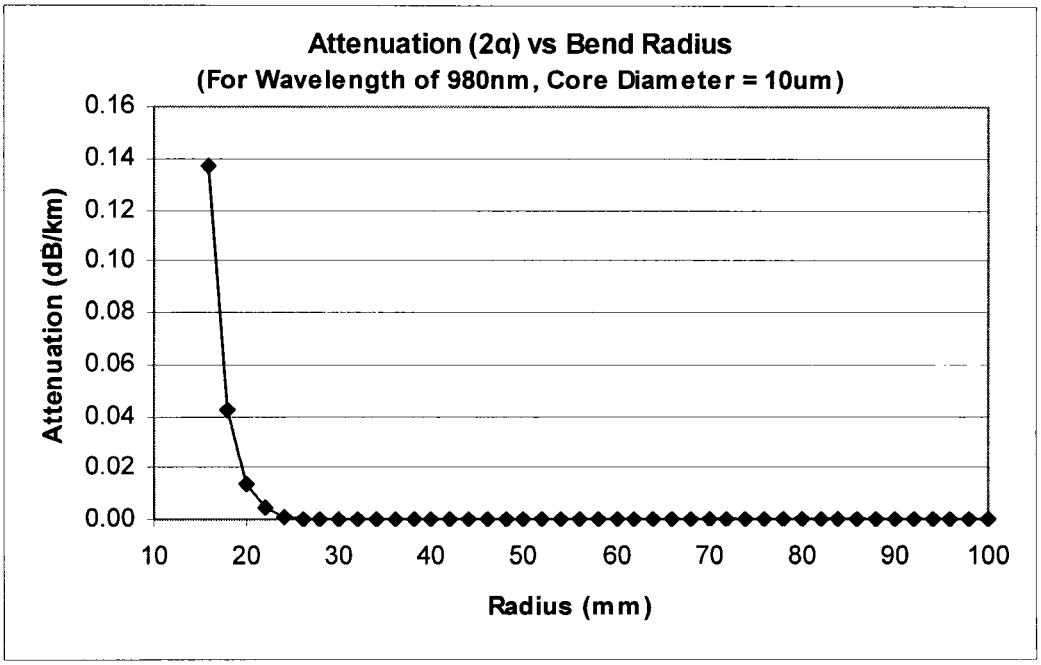

Figure 43. Attenuation for singlemode fiber with core diameter of 10um at 980nm.

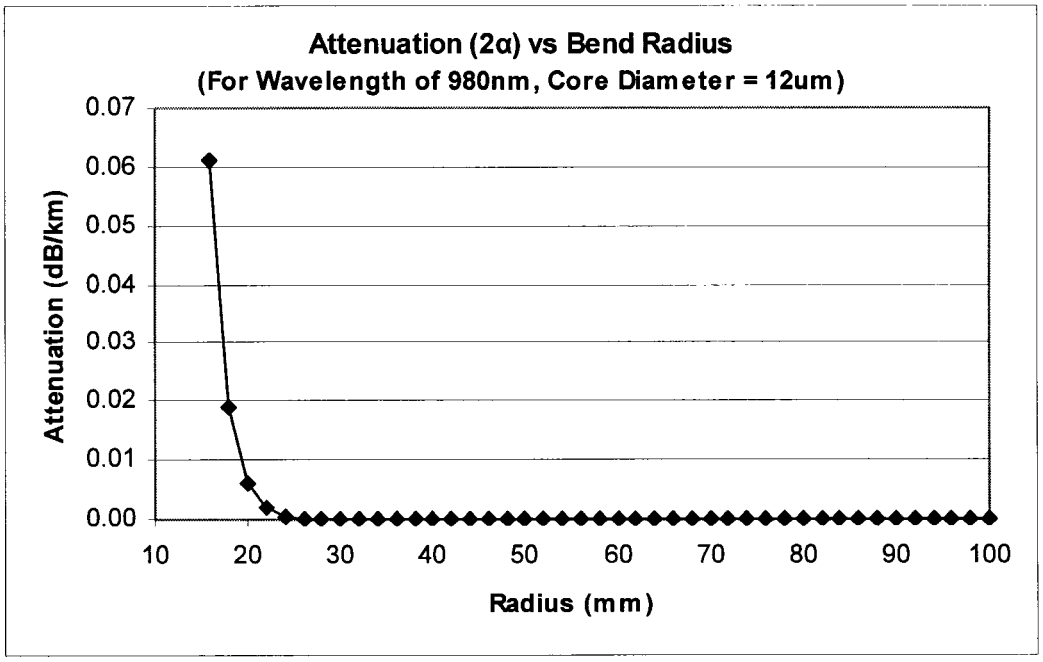

Figure 44. Attenuation for singlemode fiber with core diameter of 12um at 980nm.

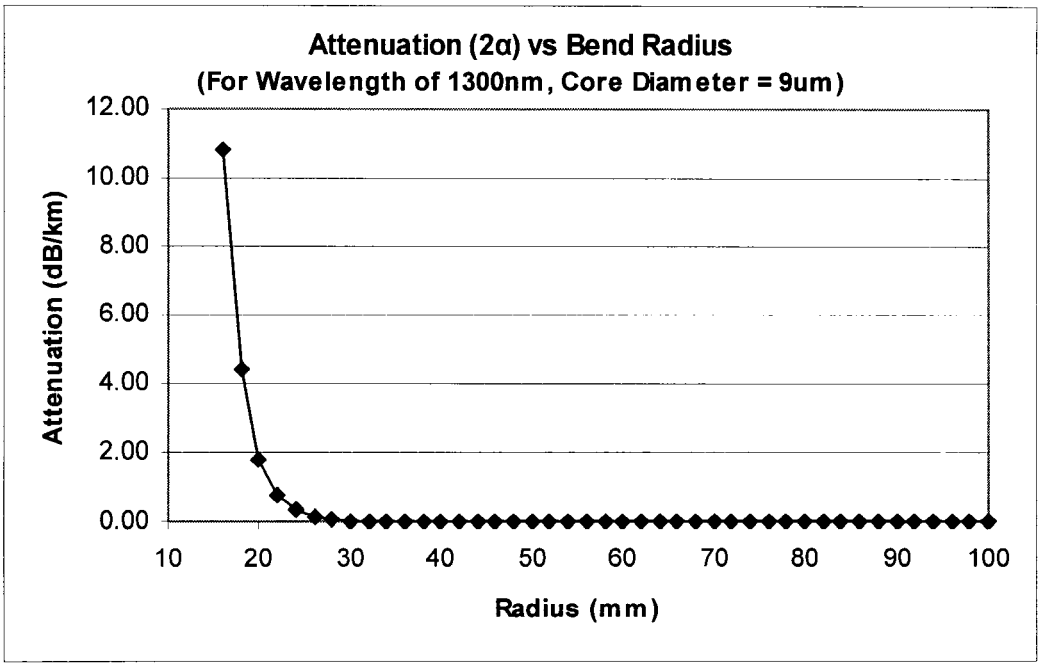

Figure 45. Attenuation for singlemode fiber with core diameter of 9um at 1300nm.

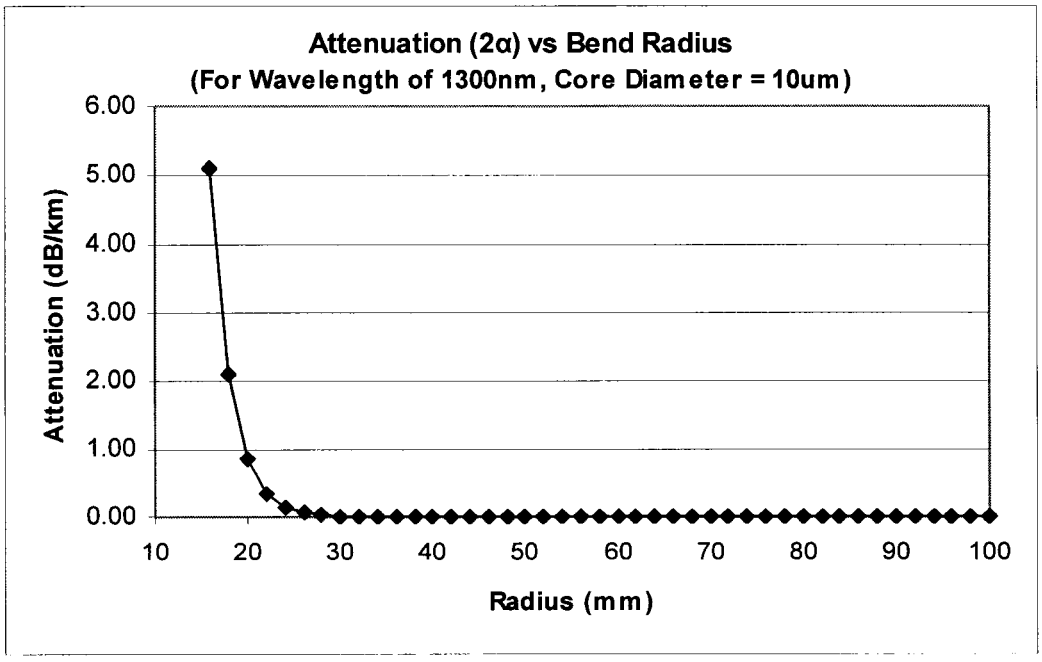

Figure 46. Attenuation for singlemode fiber with core diameter of 10um at 1300nm.

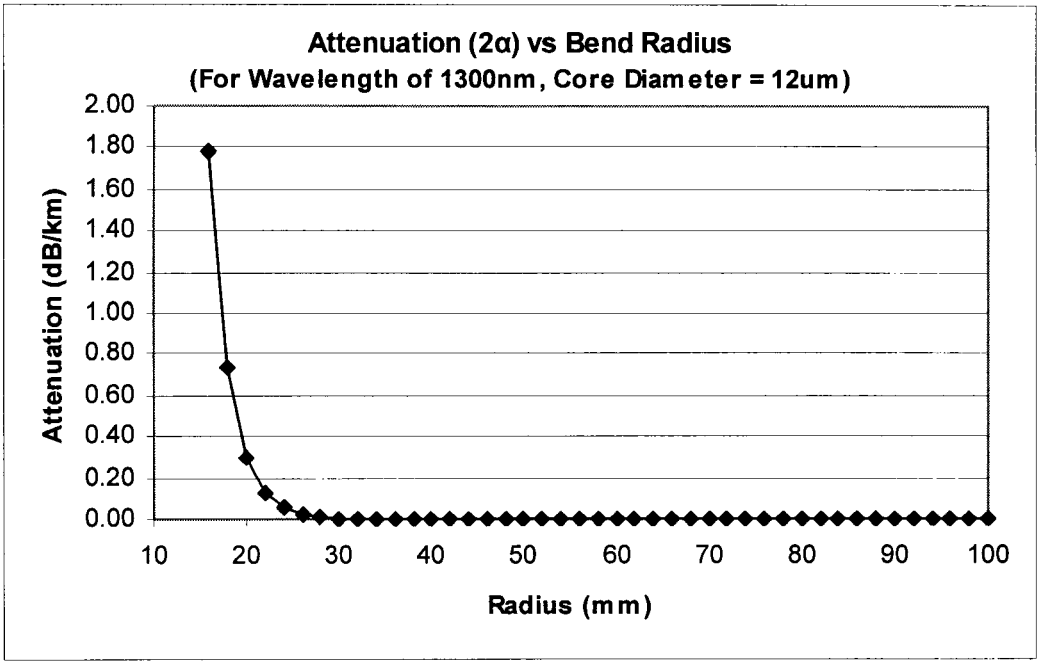

Figure 47. Attenuation for singlemode fiber with core diameter of 12um at 1300nm.

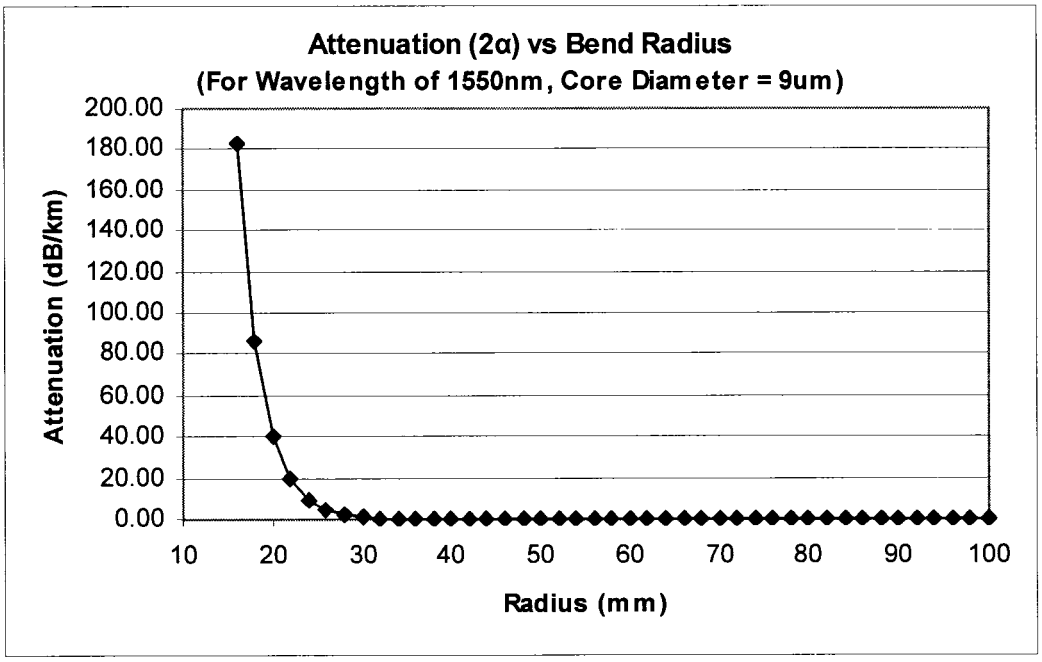

Figure 48. Attenuation for singlemode fiber with core diameter of 9um at 1550nm.

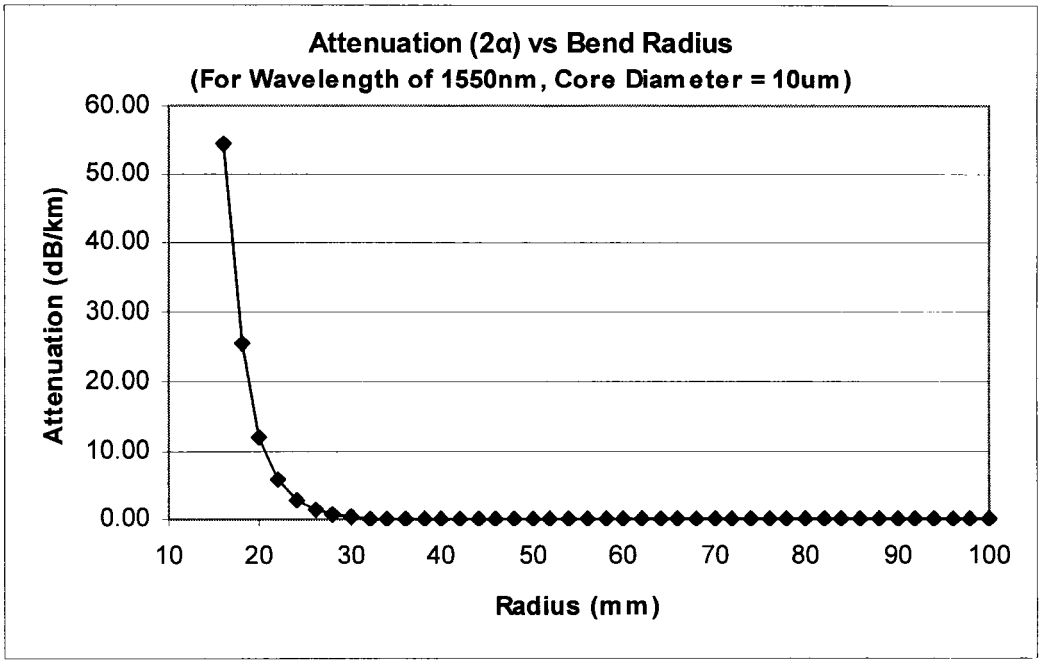

Figure 49. Attenuation for singlemode fiber with core diameter of 10um at 1550nm.

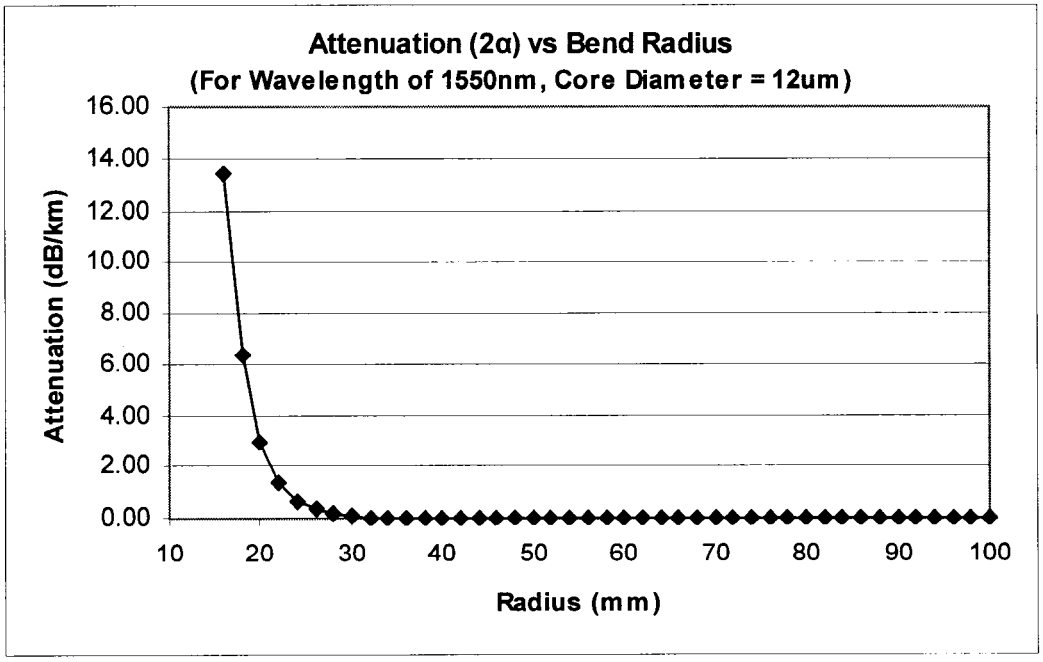

Figure 50. Attenuation for singlemode fiber with core diameter of 12um at 1550nm.

Additional changes in attenuation resulting from the change of index of refraction, other than due to the bending radius parameter, are shown below in Figures 51, 52, and 53 for wavelengths of 980nm, 1300nm, and 1550nm. The level of attenuation at 980nm is very small with a maximum peak 0.000004 dB/km at 32mm bend radius. It is small enough to be negligible; however, it is interesting to observe the attenuation behavior. The attenuation increases as bending radius decreases, i.e. the change in index of refraction increases (see Section 4.1), and reaches the maximum at 32mm then drops off to 0.000003 dB/km at minimum allowable bend radius of 16mm. From Section 4.1, the maximum change in index of refraction is at the 16mm bend radius, for all wavelengths, but this point is not the maximum attenuation change resulting from bending. The mathematical explanation could be due to the dependency on bend radius R in the (2α) equation that it is a resulting function of the exponential function of R divided by the square root function of R (see Section 1.3). The overlapping of these two functions perhaps would explain the peak irregularity that does not follow the change in index of refraction functions for all three wavelengths. The physical reason for this could perhaps be explained by that the core material enters briefly the region of non-elastic deformation at 32mm bend radius, before rupture at 16mm bend radius. Also note that the bending radius R is kept constant at 40mm, since this is the condition which gives negligible attenuation level in the prior discussed attenuation models for all three wavelengths, with no consideration for change of index of refraction at this point. In the attenuation equation, the bend radius R is chosen fixed at 40mm, then using the index change function as the driving parameter for attenuation change calculations.

At wavelength of 1300nm, the similar behavior of attenuation still occurs, but with smaller change and at a different bend radius condition. The attenuation change is a maximum at a bend radius of 24mm with 0.010360 dB/km and is 0.009599 dB/km at the minimum allowable bend radius of 16mm. These levels of attenuation are again small and negligible. At 1550nm wavelength, the similar attenuation behavior of the peak not being at the maximum change of index of refraction still exists, but is negligible compared to the magnitude of the overall attenuation as the function of bend radius. The overall attenuation here at 1550nm is relevant, with a magnitude about 6 dB/km at 16mm bend radius, that decreases to less than 1 dB/km at 1000mm bend radius. The attenuation would eventually come to zero with a bend radius that goes to infinity, or unbent condition.

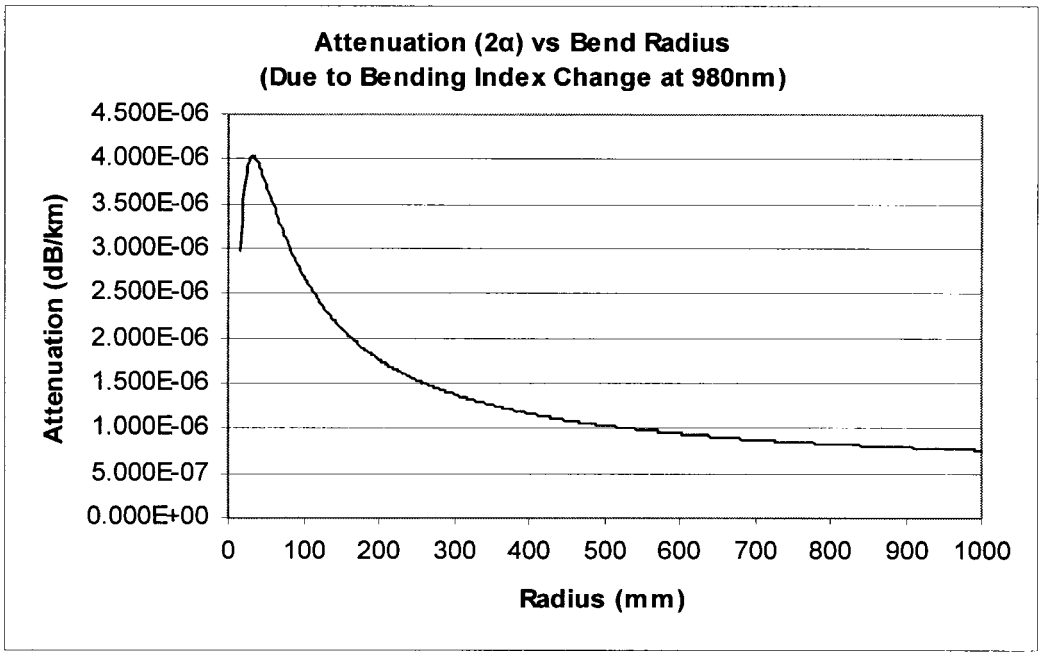

Figure 51. Attenuation due to index change resulting from bending at 980nm.

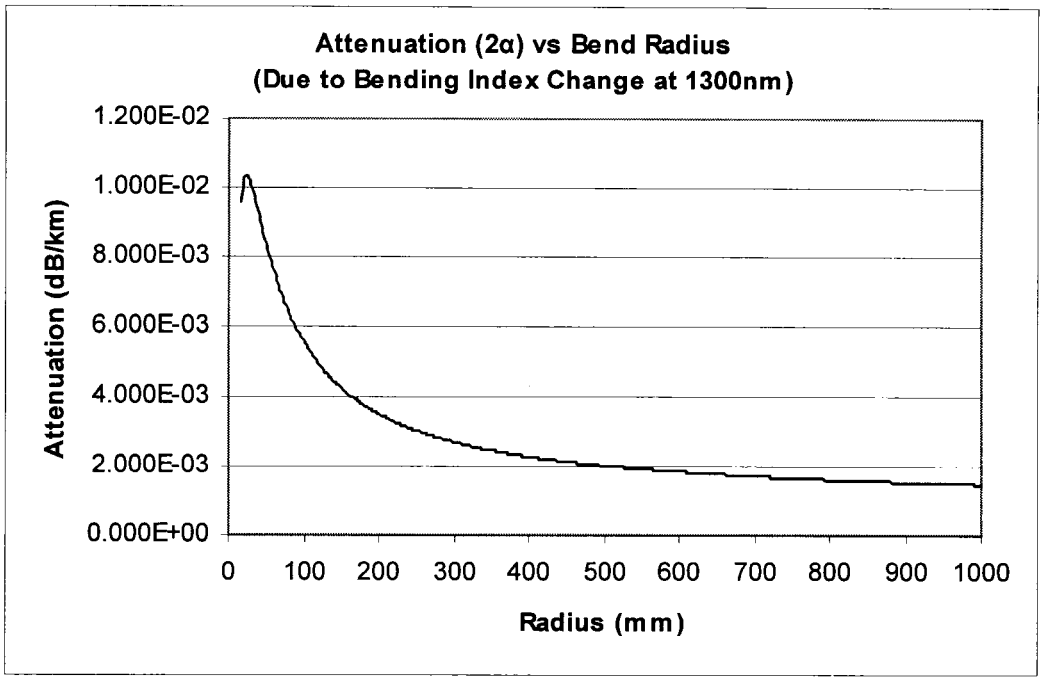

Figure 52. Attenuation due to index change resulting from bending at 1300nm.

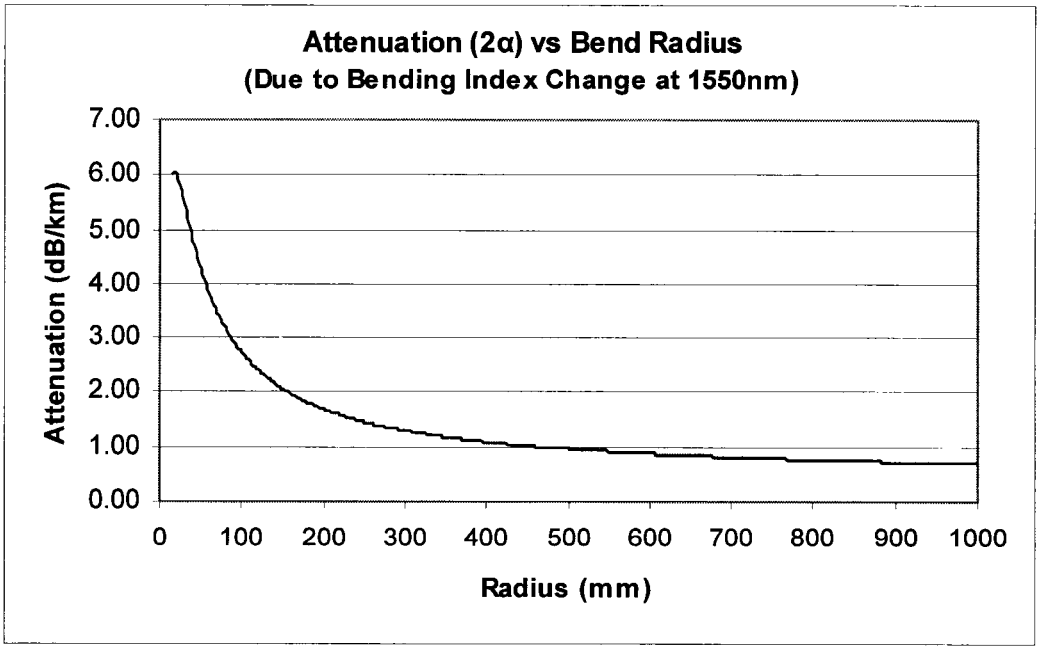

Figure 53. Attenuation due to index change resulting from bending at 1550nm.

The change in attenuation due to temperature effects is purely dependent upon the change of index of refraction of fused silica with temperature. With the reference temperature at 25°C, the attenuation at 25°C is 0.436 dB/km, and the change in index of refraction is 0.013630 from 25°C to 1000°C, and this refractive index change results in a change in attenuation of 0.000345 dB/km and 0.137 dB/km for 1300nm and 1550nm wavelengths, respectively. Figures 54 and 55 show the attenuation results for these conditions. The comparison is made between two wavelengths of 1300nm and 1550nm to show the characteristic that the attenuation is more significant with higher wavelengths. It is noticeable that the slopes of the attenuation curves change more at higher temperatures than lower temperatures; but the overall slopes of the curves follow much of the linear relationship with temperatures from 25°C to 600°C.

The attenuation change due to thermal stress contributes in cases of the thermal coefficient mismatch between the core and cladding, used when fiber strengthening is implemented (see Section 1.9). It is negligible at a wavelength of 1300nm - it is approximately 0.000910 dB/km. At 1550nm, the attenuation change level is more relevant at 0.436 dB/km. Figures 56 and 57 show these results of attenuation change due to temperature. The slopes of the curves represent the rate of change and they hold a linear relationship with temperature, since thermal stress is resulting from the difference in temperature in terms of mismatch in thermal coefficients of expansion. The thermal expansion of fused silica has quite a linear relationship at higher temperatures. The results, however, do reaffirm the trend of higher attenuation change occurs at higher wavelengths.

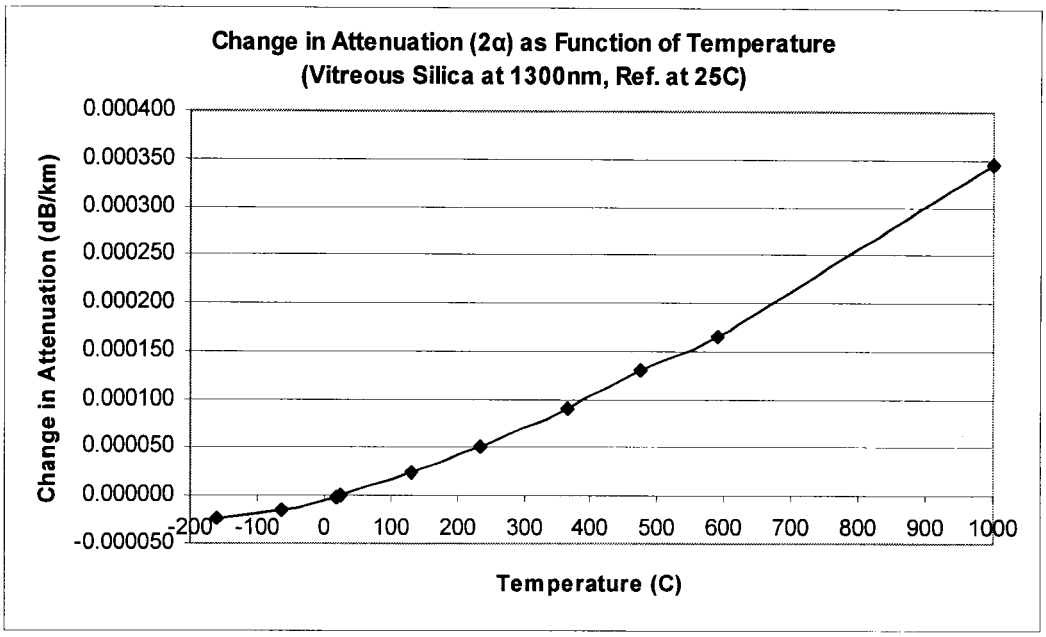

Figure 54. Change in attenuation as function of temperature at 1300nm.

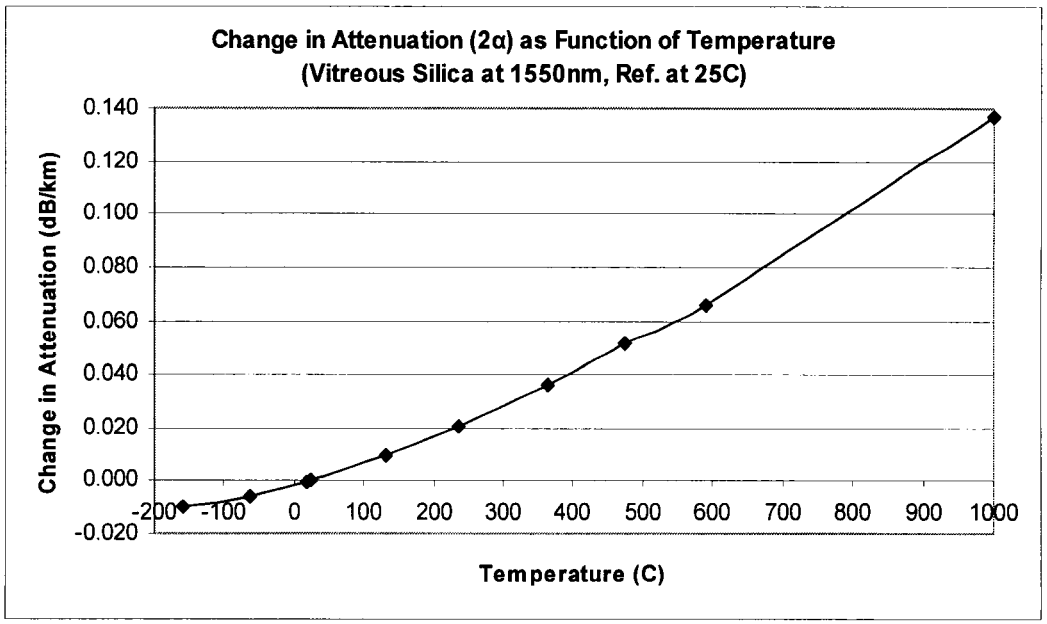

Figure 55. Change in attenuation as function of temperature at 1550nm.

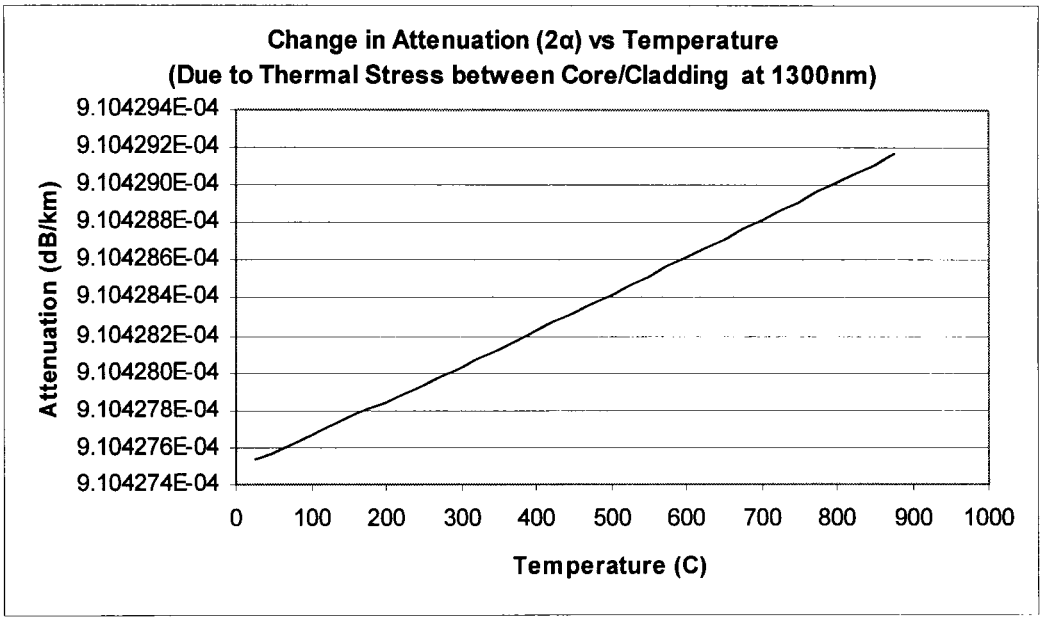

Figure 56. Change in attenuation resulting from thermal stress at 1300nm.

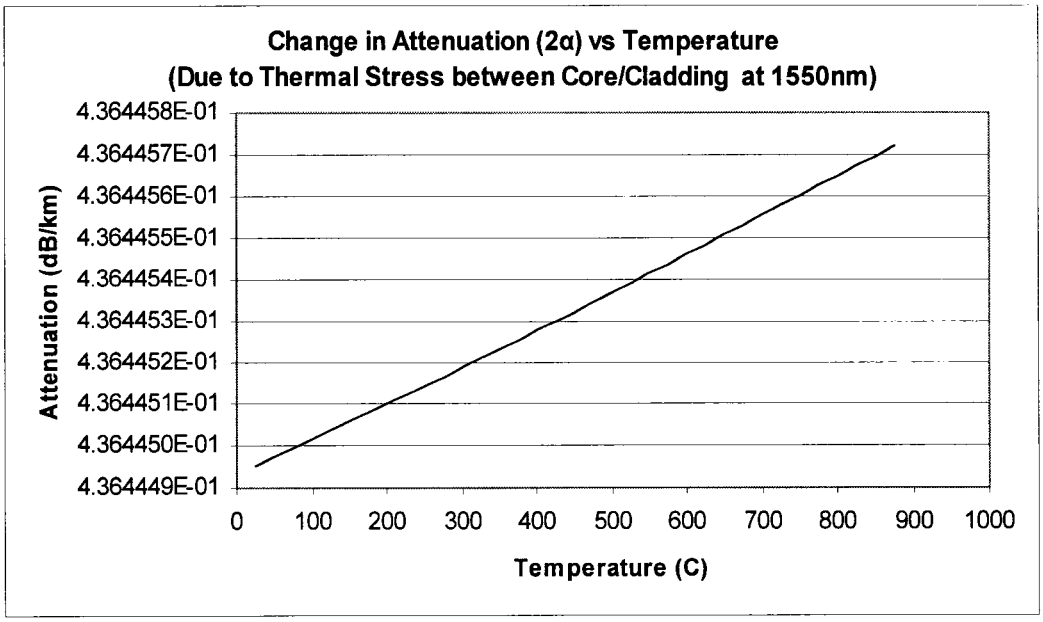

Figure 57. Change in attenuation resulting from thermal stress at 1550nm.

4.3 Dispersion change with bending and temperature

Total dispersion is the sum of both the material dispersion and the waveguide dispersion. Material dispersion depends on index of refraction as a function of wavelength, and it has zero value at a wavelength of 1270nm and becomes negative beyond that. Waveguide dispersion, on the other hand, is dependent on the V parameter function, also known as the propagation constant. More details discussion is covered in Section 1.4.

Dispersion in this calculation is considered as waveguide dispersion, unless noted. Dispersion is calculated for three wavelengths of 980nm, 1300nm, and 1550nm. Their V numbers are calculated using a fiber core radius of 4um, Δ of 0.2%, and the index of refraction at that particular wavelength. Dispersion values are -16.906 ps/km*nm, -8.943 ps/km*nm, and -8.452 ps/km*nm for 980nm, 1300nm, and 1550nm, respectively. These dispersion values are for unbent fiber and used as reference values for calculating the percent change in waveguide dispersion, when introducing the change of index of refraction as the result of fiber bending and temperature function.

Dispersion change as the result of the change in index of refraction is calculated to be largest at the 16mm bend radius of -15.546 ps/km*nm for 980nm, -9.084 ps/km*nm for 1300nm, and -8.482 ps/km*nm for 1550nm wavelength. These dispersion change values decrease to very small amount as the bending radius increases and stabilized to the reference values shown above. These are shown in Figure 58. The percent difference in change of dispersion is calculated for all three wavelengths. The biggest change is 8.04% at 1550nm, then 1.57% at 1300nm, and 0.35% at 980nm wavelength. The percent

change from the unbent condition is plotted in Figure 59 for three wavelengths.

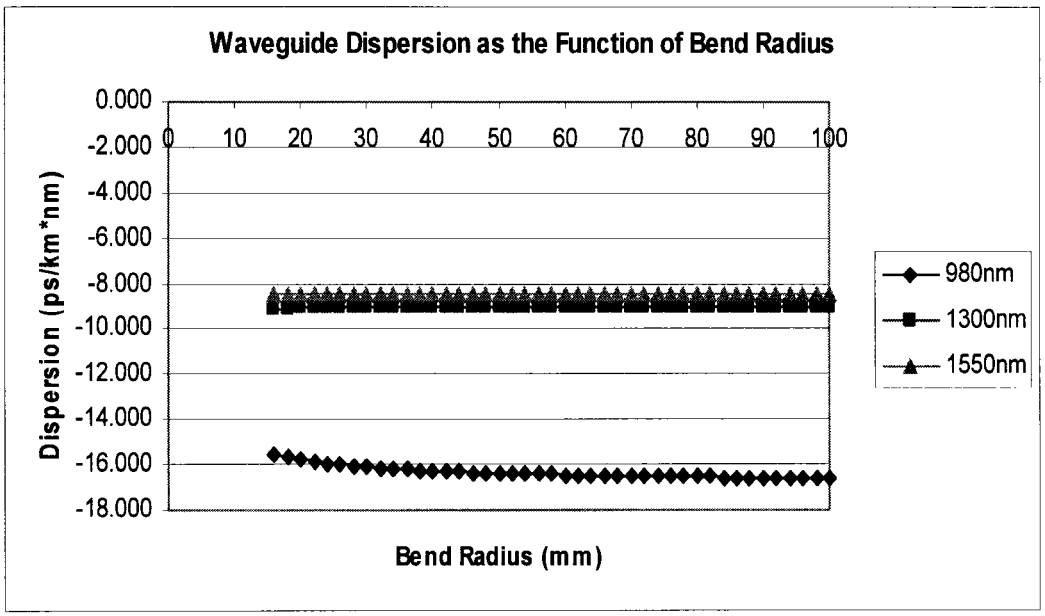

Figure 58. Waveguide dispersion as function of fiber bend radius.

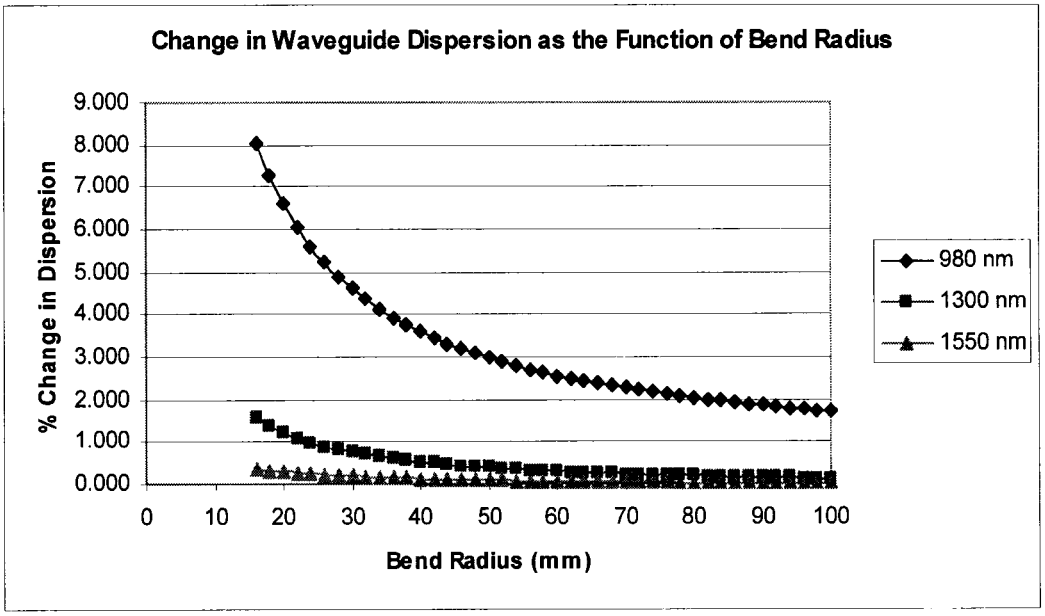

Figure 59. Change in waveguide dispersion as function of fiber bend radius.

Waveguide dispersion is calculated to be -16.858 ps/km*nm, -8.938 ps/km*nm and -8.445 ps/km*nm at 25°C for 980nm, 1300nm and 1550nm, respectively. The change of dispersion with temperature, referenced to 25°C, is small with 0.37% change in dispersion at 1000°C with a wavelength of 1300nm, and 0.12% change at 1000°C with a wavelength of 1550nm. However, at 980nm, the change of dispersion at 1000°C is about 1.77%, which is not totally negligible. It is observed that waveguide dispersion is more sensitive to change of temperature at lower wavelengths than at higher wavelengths. For telecom wavelength range of 1300nm to 1600nm, the waveguide dispersion change is small of less than 0.5% that is due to temperature. Figures 60 and 61, show the variation of waveguide dispersion with temperature for 980nm, 1300nm and 1550nm wavelengths and their percent differences relative to temperatures.

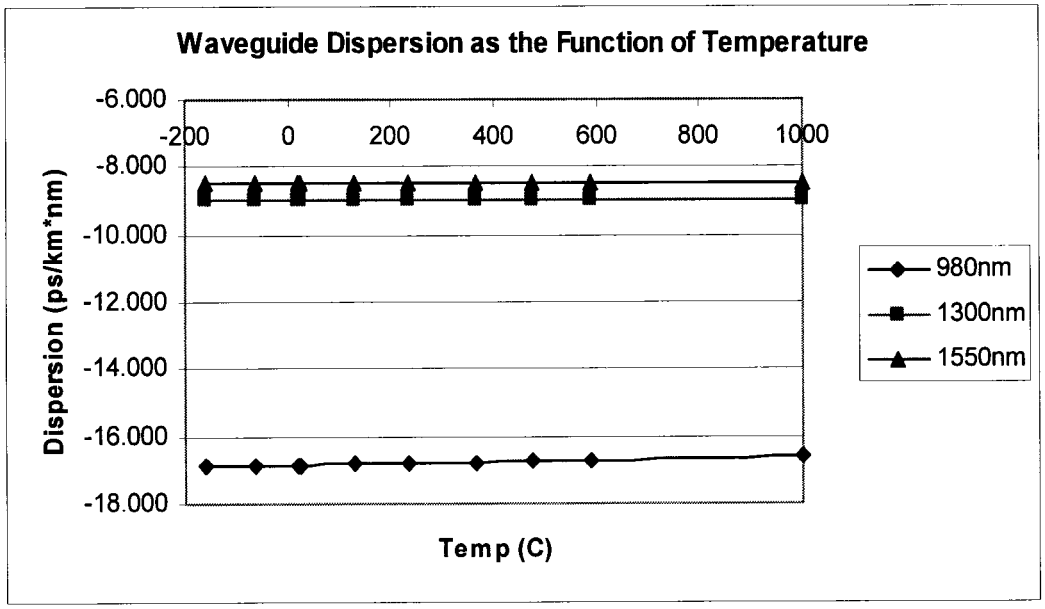

Figure 60. Waveguide dispersion as function of temperature for various wavelengths.

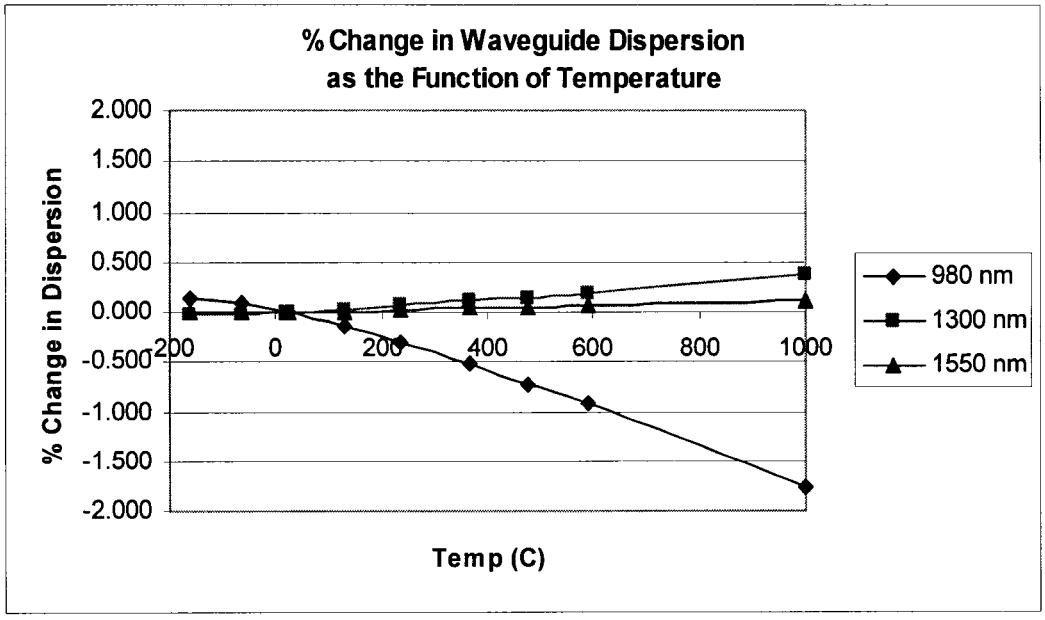

Figure 61. Change in waveguide dispersion as function of temperature.

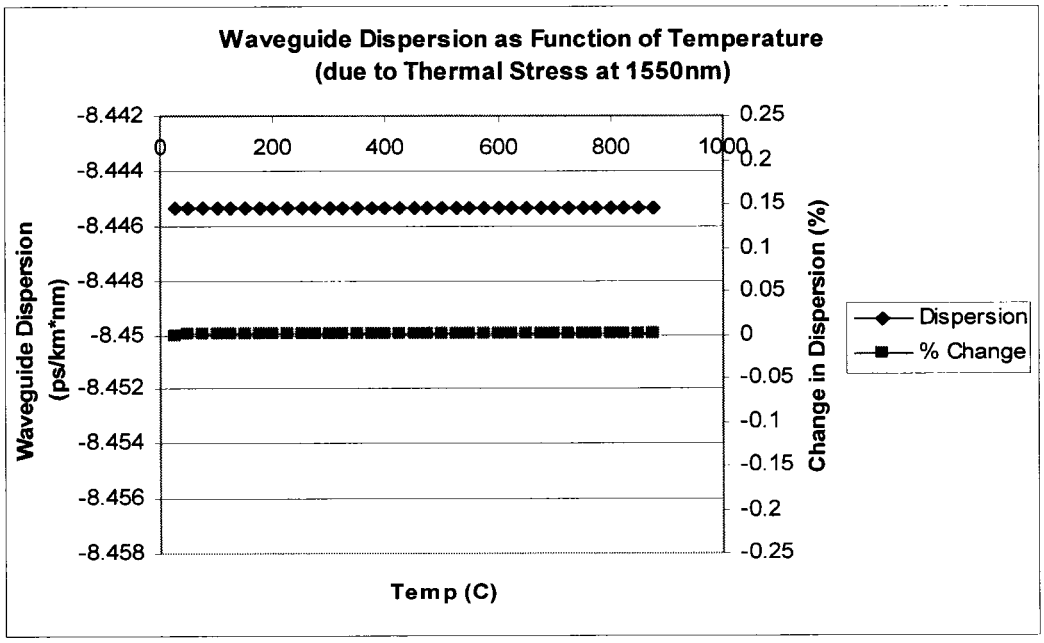

Figure 62. Waveguide dispersion resulting from thermal stress at 1550nm.

The additional change of waveguide dispersion due to thermal stress resulting from coefficient of thermal mismatch between the core and cladding is calculated to be -8.445 ps/km*nm from 25°C to 875°C. This is a very small change (2.5E-8 %) in dispersion and is negligible. The result is shown in Figure 62 and is assumed to be the applying trend for all wavelengths.

4.4 Birefringence change with bending and temperature

Birefringence due to bending of fibers is calculated for three wavelengths of 980nm, 1300nm, and 1550nm. There are two components involved with birefringence; one that is bending induced and the other is the tension component birefringence that is added to result in the total birefringence. Figures 63, 64, and 65 below show the curves of β_b, β_{tc}, and β_{total} for 980nm, 1300nm, and 1550nm. Bb is the bending induced birefringence, β_{tc} is the tension component birefringence, and β_{total} is the sum of the other two effects. At the minimum allowable bending radius of 16mm, the total birefringence for 980nm is -0.219 rad/m, -0.164 rad/m for 1300nm, and -0.137 rad/m for 1550nm wavelength. Note that the worst case is -0.219 rad/m (equivalent of 12.540 deg/m) at wavelength of 980nm which is still a quite good total birefringence level, since birefringence less than 10 deg/m is considered quite well in circularity of the fiber. This circularity is recognized by Okoshi and Kikuchi [28] in their work. A more detail discussion of characteristics of birefringence is covered in Section 1.5 of this research paper.

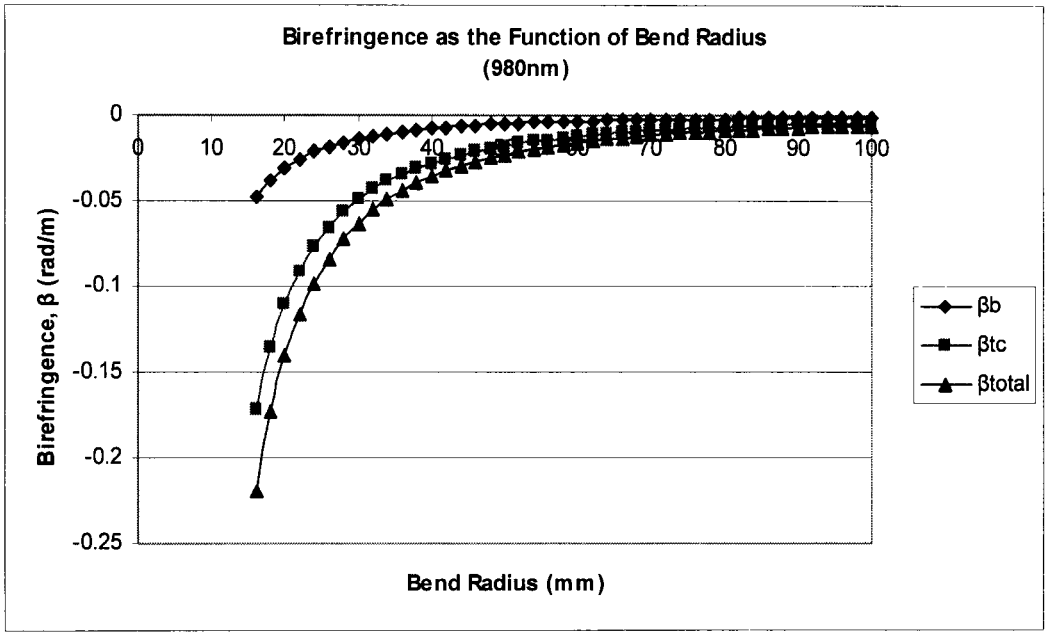

Figure 63. Birefringence as the function of fiber bend radius at 980nm.

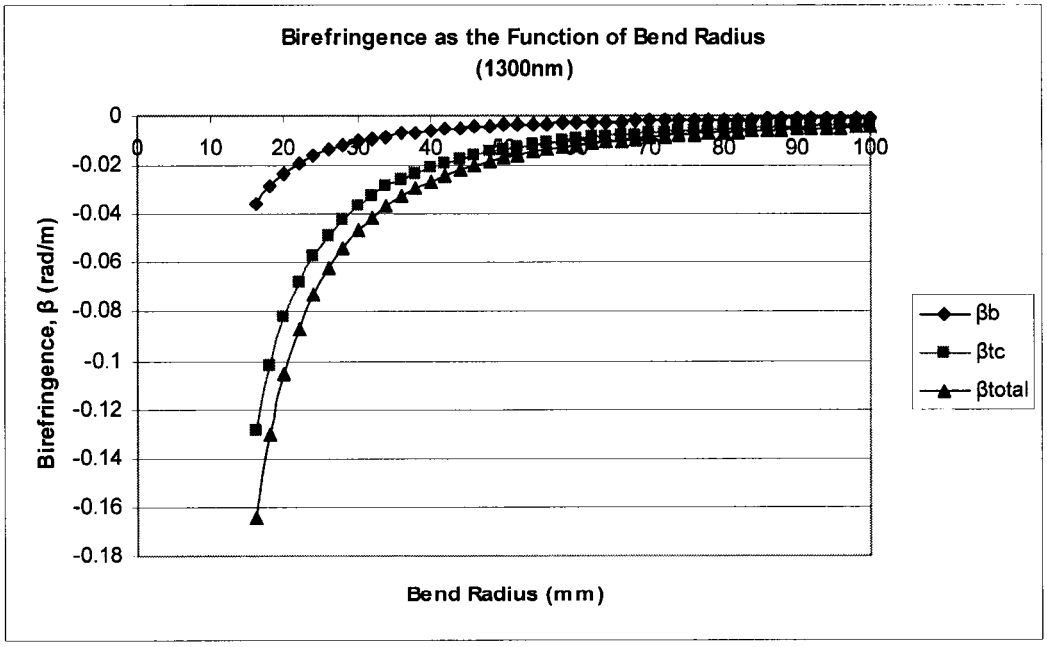

Figure 64. Birefringence as the function of fiber bend radius at 1300nm.

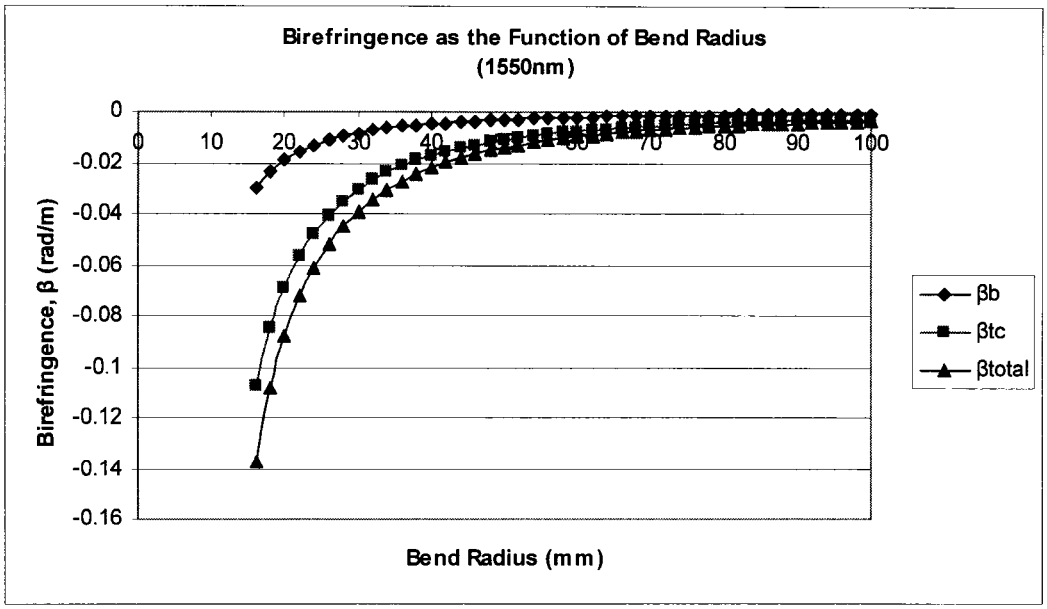

Figure 65. Birefringence as the function of fiber bend radius at 1550nm.

Temperature dependence of birefringence is considered by the change of index of refraction of fused silica with temperature, and this in turn changes the strain optic coefficient, Cs (see Section 1.5), that would result in a change in birefringence. Note that if only temperature is involved, it is considered to use β_b relationship to show this effect. Figure 66 shows the birefringence of -0.0012214 rad/m, -0.0009136 rad/m, and -0.0007616 rad/m for three wavelengths of 980nm, 1300nm, and 1550nm, respectively, at temperature of 25°C. These levels of birefringence are small and negligible, but what is more important is the trend line. The birefringence trend seems to be increasing with the increase in temperature in the negative rotation direction, but nevertheless, the birefringence at lower wavelengths is more sensitive to temperature than at longer wavelengths.

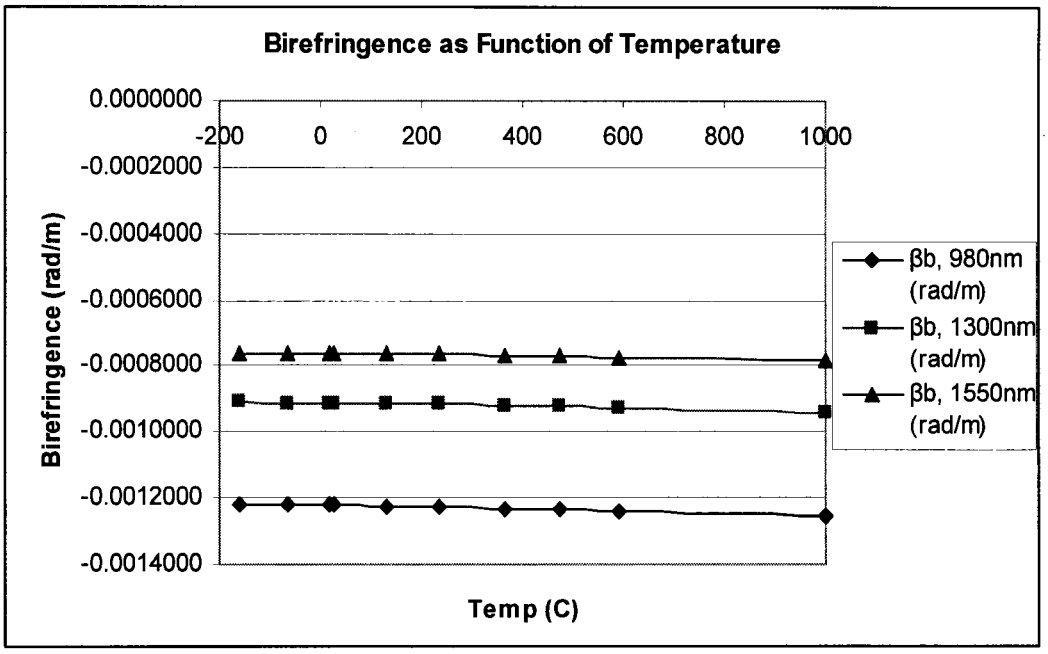

Figure 66. Birefringence as function of temperature for different wavelengths.

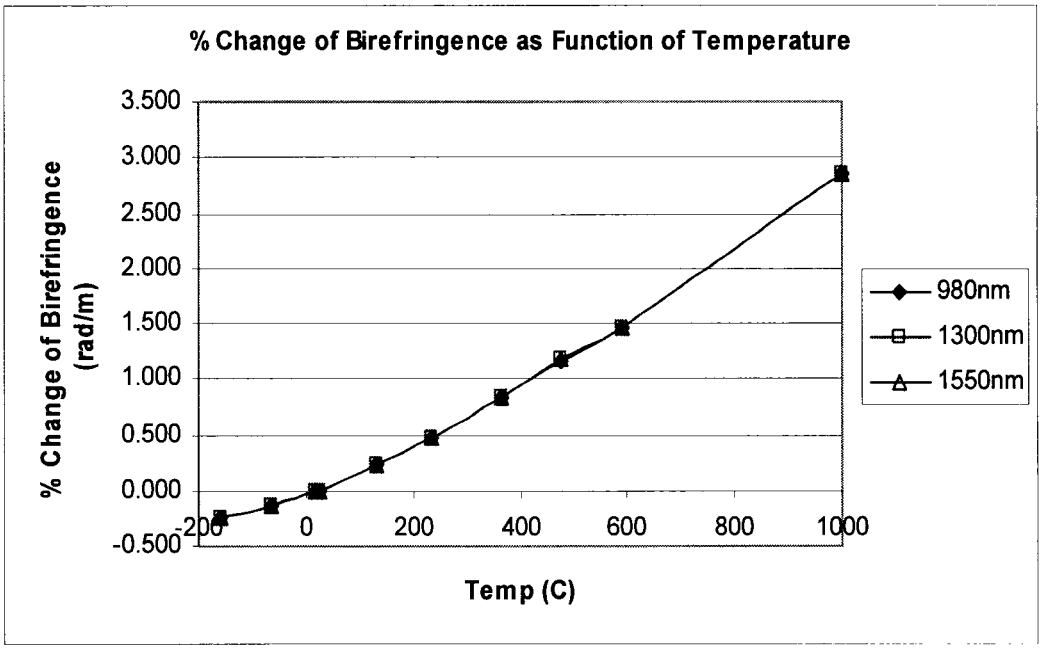

Figure 67. Change of birefringence as function of temperature for different wavelengths.

Figure 67 shows the percent change in birefringence as a function of temperature for all wavelengths with referenced to 25°C. The change in birefringence is quite consistent for all wavelengths calculated. Over the range of 1000° C, from room temperature at 25°C, the percent change of birefringence is about 2.85 percents.

The change of birefringence due to additional thermal stress on fiber with different core and cladding materials is shown in Figure 68. There is basically no change of birefringence or negligible amount due to thermal stress on fiber at a detectable and meaningful level. The trend shows an increase in birefringence with temperature, and it seems change linearly from temperature of 300°C to 900°C. The birefringence seems to change less and reaches a plateau level at some higher temperature than 900°C shown. This is calculated and shown for wavelength of 1550nm, but is assumed to be same for all wavelengths.

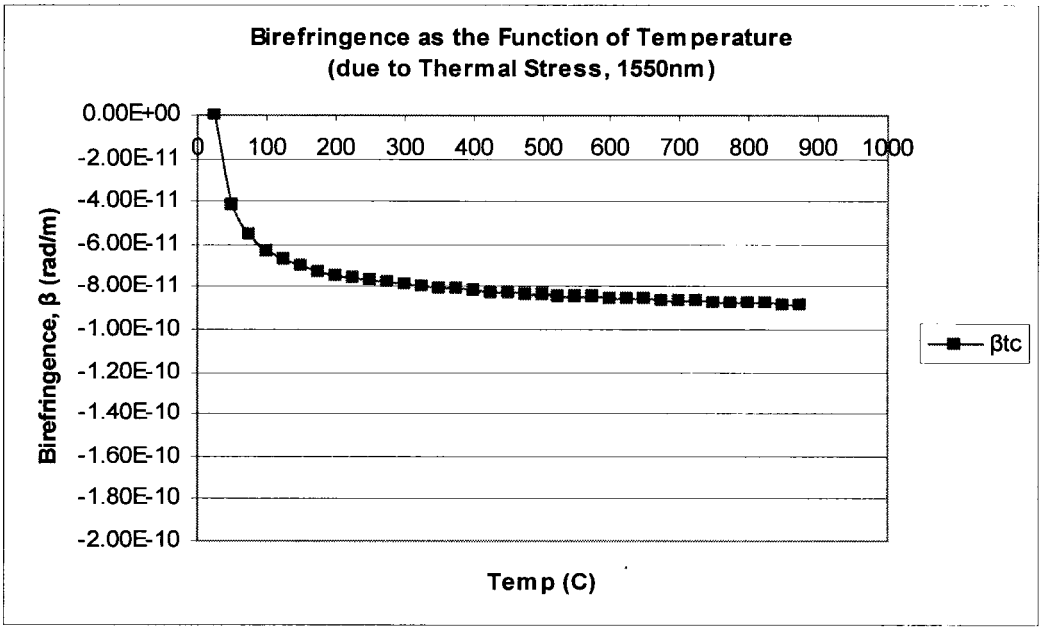

Figure 68. Birefringence as function of temperature due to thermal stress effect.

4.5 Fiber Bragg grating properties change with strain and temperature

Fiber Bragg grating (FBG) scope in this study is considered as a single grating element, and is analyzed for its behavior change due to stress - strain effect and temperature effect. The Bragg grating is normally inscribed into the core glass; thus it is assumed here to experience the same stress – strain effect resulting from bending of optical fiber. There is thought to be a coupling factor between the sensor and the fiber, and it is not being addressed in this research. Future experiments with empirical data can help better explain this topic.

FBG sensitivities to strain and temperature are independent effects and can be added together to get the total effect for the grating as sensor, since the grating is sensitive to both strain and temperature. Figure 69 shows the change in Bragg grating wavelength as a function of the bend radius. For grating's centering wavelengths of 980nm, 1300nm, and 1550nm, the change is 0.515 nm, 0.680 nm, and 0.808 nm, respectively, at the bending radius of 16mm. As the fiber bending radius increases to infinity, or unbent condition, the Bragg grating wavelength change returns to zero value. The grating sensitivity is calculated to show how much change of the grating wavelength due to the strain level for which is resulted from fiber bending. Fiber Bragg grating sensitivity of 0.00206 nm/ustrain for 980nm center wavelength, and increases to 0.00272 nm/ustrain for 1300nm, and 0.00323 nm/ustrain for 1550nm center wavelength grating. These levels of sensitivity for the grating are quite high theoretically, in the picometers range, and may only be limited in real application by electronics setup. Figure 70 shows this strain sensitivity and the grating period as a function of wavelength.

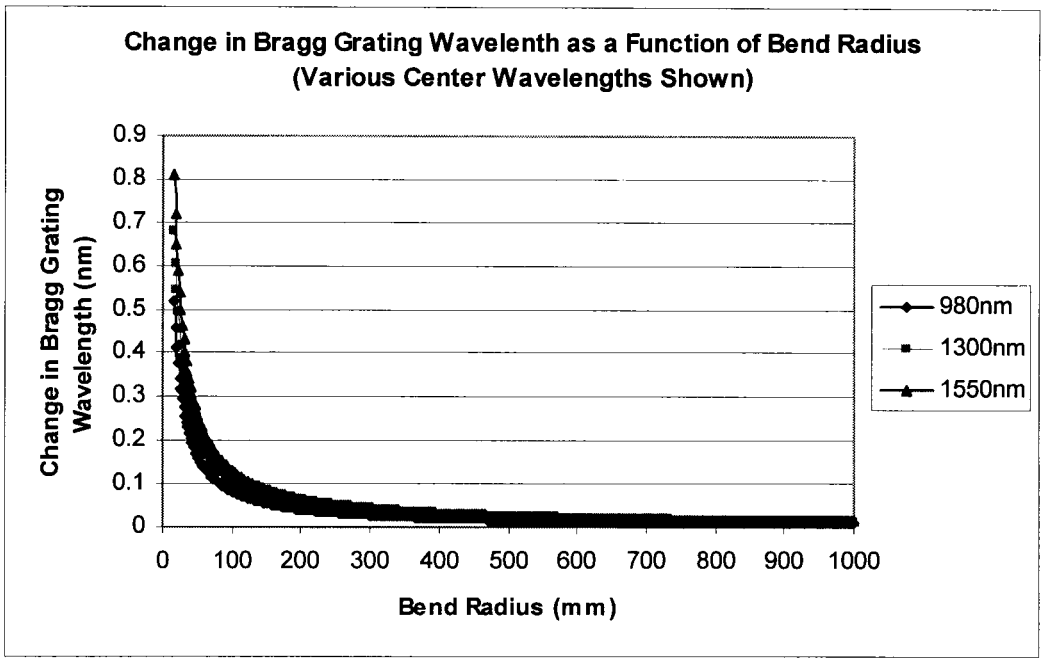

Figure 69. Change in Bragg grating wavelength as function of fiber bend radius.

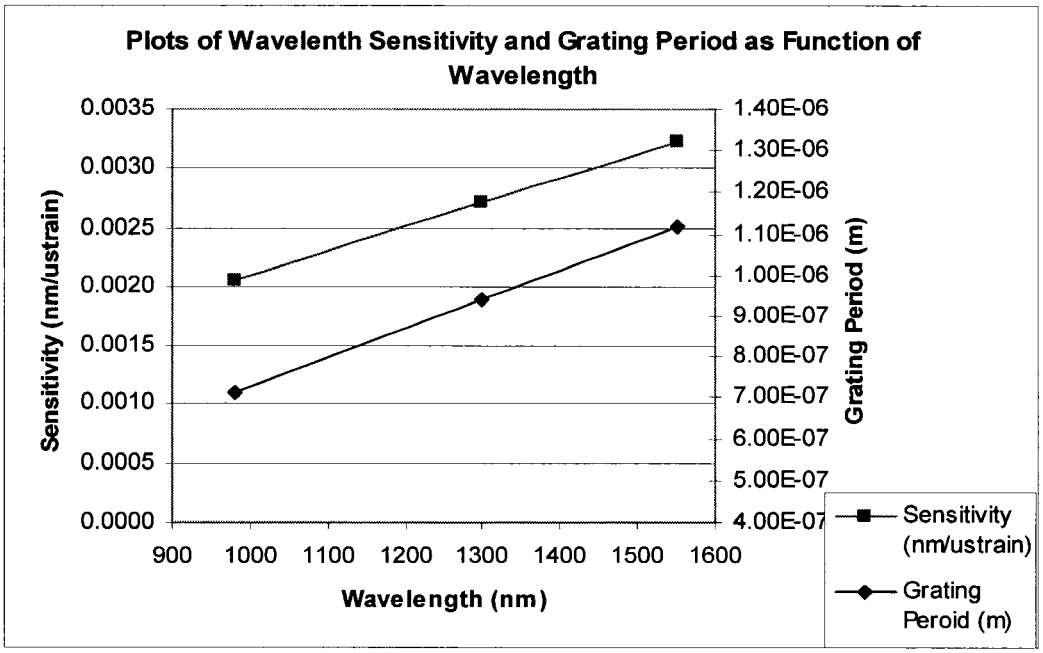

Figure 70. Plot of wavelength sensitivity to strain and grating period as function of wavelength.

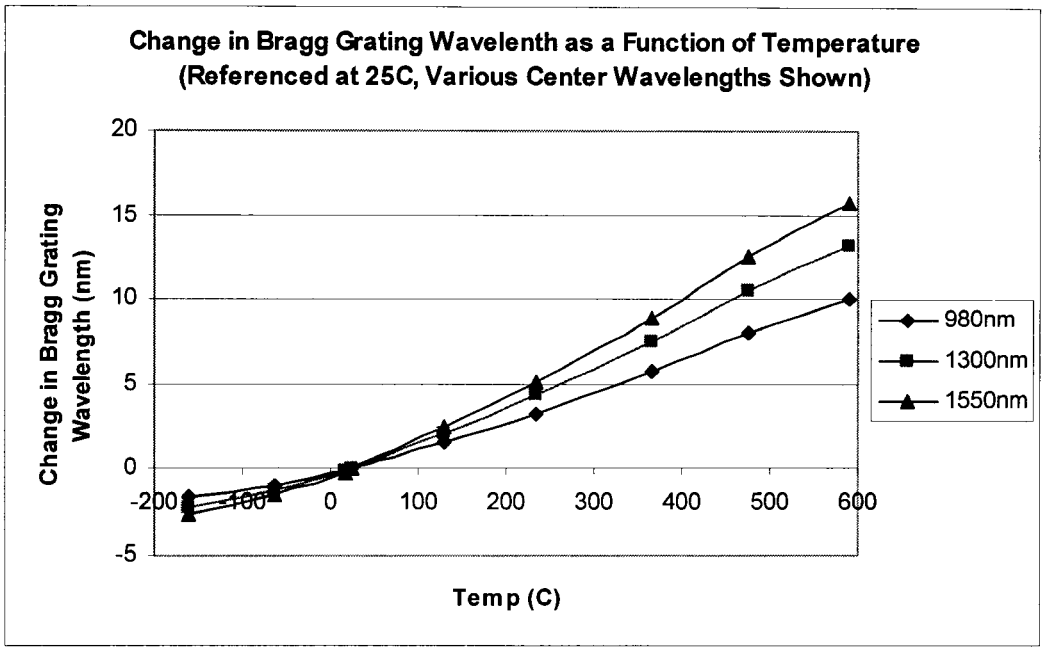

Figure 71. Change in Bragg grating wavelength as function of temperature.

Bragg grating temperature dependency lies mainly in change of the index of refraction of core material due to temperature. In the Figure 71, it is observed that the change in Bragg grating wavelength is much larger due to temperature than strain in magnitude, comparing to Figure 69. The data are referenced to 25°C (room temp), and they show the change of 9.96 nm, 13.18 nm, and 15.69 nm for 980nm, 1300nm, and 1550nm centering wavelengths at 600°C, respectively. The sensitivity of the grating with temperature is shown in Figure 72, with fitted lines over the data. The reference data points at 25°C should be ignored because they show no strain at unstressed condition, and thus resulting in no sensitivity. The sensitivity for temperature below the reference temperature of 25°C needs to be corrected for grating experience of compression due to temperature drop, and is not corrected here. The trend seems to show increasing

sensitivity with temperature with 0.016 nm/C, 0.022 nm/C, and 0.026 nm/C for 980nm, 1300nm, and 1550nm centering wavelengths at 600C, respectively. Lower wavelengths also have higher sensitivity than higher wavelengths.

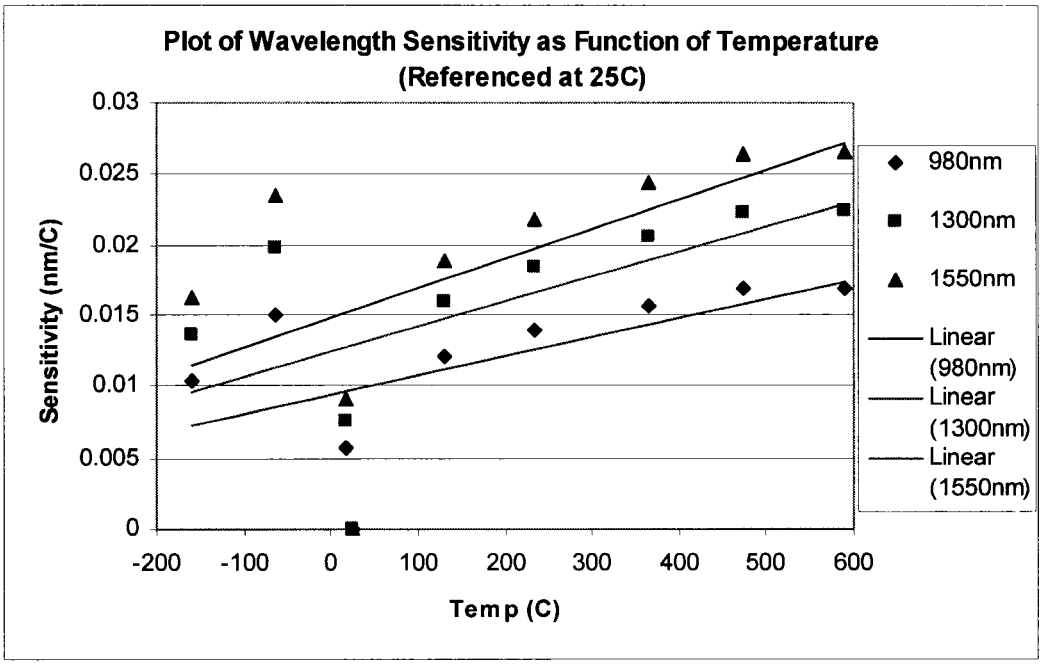

Figure 72. Plots of Bragg grating wavelength sensitivity as function of temperature.

CHAPTER 5

Conclusions

The effects of stress – strain and temperature on singlemode fibers are relevant because they introduce signal degradation to the optical signal. Optical properties like attenuation, dispersion and polarization, in terms of birefringence, are related to the effect of change in index of refraction of fused silica glass fiber due to external forces caused by stress and temperature. The additional effect of thermal stress has been examined for special cases where strengthening of the fiber is done, with a higher thermal coefficient of expansion material in the cladding. When stress is introduced through bending, the index of refraction decreases as the bending radius gets smaller. The limit allowable bend radius is 16mm, before the fiber breaks. Temperature also makes the index of refraction to change. This effect is primarily on the optical property of fused silica; its index of refraction decreases with temperature increase. In the case where thermal stress exists, it creates additional tensile stress on the core, and this stress has the same effect as the bending stress, which would decrease the index of refraction as well.

The modeling result of the fiber core bending using the finite element analysis agrees reasonably with that of the beam analytical solution. It gives an accuracy of about 15% at 16mm bend radius, comparing to that of the analytical beam bending model. The best case is 0.26% at 40mm bend radius, where the maximum principal stress level is lower at the larger bend radius condition. The error in the results can be improved by using a hexagonal element type and finer elements in the model. This would require longer computational time to run the finite element model.

The attenuation increases with decreasing index of refraction and decreases (improvement in attenuation) with the increase in core diameter. Optimization can be done when designing a specific fiber for a defined optical network. Attenuation is also more sensitive to change in index of refraction at higher wavelengths than at lower wavelengths for the same other conditions. Attenuation change due to temperature effects are small and negligible, and that due to thermal stress is about 8% of that compared to maximum bending condition.

Material dispersion depends on material properties and is a function of wavelength. Waveguide dispersion on the other hand changes with the change of index of refraction and temperature. Waveguide dispersion increases as the index of refraction decreases and with a larger magnitude at lower wavelengths than higher wavelengths. Temperature effects on waveguide dispersion is small at higher wavelengths, with a worst case change of less than 2%, but still follows the same behavior of larger dispersion magnitude at lower wavelengths. Thermal stress effect on waveguide dispersion is small and negligible.

Birefringence change due to bending is higher with larger change in index of refraction and is also higher change at lower wavelengths than higher wavelengths. The effect of temperature on birefringence is small and negligible, though it has a higher magnitude at lower wavelengths than higher wavelengths. The change due to temperature effect on birefringence is about the same for all wavelengths, with a reference to room temperature, the change is about 3% at 1000°C. The effect of thermal stress on birefringence is negligible.

Fiber Bragg grating strain sensitivity change is higher for larger change in index of refraction, and the sensitivity change is also higher at higher grating centering wavelengths, which is the design parameter for the grating in manufacturing. Grating period is also larger for a higher centering wavelength. Temperature sensitivity of fiber Bragg grating is about 8 times higher compared to that of strain sensitivity, for all wavelengths calculated.

CHAPTER 6

Recommendations for Future Research

The focus of this research topic is on the effect of bending and temperature on optical signal degradation, primarily attenuation, dispersion, and birefringence in step-index singlemode fibers. The scope can be extended to include other optical parameters that are also important in designing the optical system network and different complex waveguide geometries of different index profiles. Multimode fibers would also be an exciting area of research extension, since it is more widely used for shorter transmission distance like metro network applications and are also more economically favored.

The other part that is important as the extension of this work is to design experiments to provide the verification work of the models with empirical data. It was motivated at first to include that as part of this analytical work, but the equipment issues came up and therefore it redefined the objectives of the research effort. This part would be complemented well for confirming the models and also would provide an exciting opportunity for experimentation.

References

1. P. Green Jr., Fiber Optic Networks, (Englewood Cliffs: Prentice Hall, 1993) p.36.

2. D. Halliday, R. Resnick, Fundamental of Physics, Third Edition Extended, (New York: John Wiley & Sons, 1988) p.868.

3. C. Kao, Optical Fiber Systems: Technology, Design, and Applications, (New York: McGraw-Hill, 1982) p.33.

4. W. W. Morey, G. Meltz, W. H. Glenn, "Fibre Optic Bragg Grating Sensors", Proceeding of SPIE, **1169** 98 (1989).

5. M. G. Xu, L. Reekie, Y. T. Chow, J. P. Dakin, "Optical In-fibre Grating High Pressure Sensor", Electronic Letters, **29** 398 (1993).

6. I. Bennion, J. A. R. Williams, L. Zhang, K. Sugden, N. J. Doran, "Tutorial Review, UV-Written In-Fibre Bragg Gratings", Optical and Quantum Electronics, **28** 93 (1996).

7. D. Parmar, D. R. Sprinkle, J. J. Singh, "Development of In-Fiber Reflective Bragg Gratings as Shear Stress Monitors in Aerodynamic Facilities", National Aeronautics and Space Administration, (1998).

8. G. P. Agrawal, Nonlinear Fiber Optics, (Boston: Academic Press, 1989) p.6.

9. J. P. Powers, An Introduction to Fiber Optic System, (Boston: Irwin, 1993) p.49.

10. P. Green Jr., Fiber Optic Networks, (Englewood Cliffs: Prentice Hall, 1993) p.49.

11. L. Lewin, "Radiation from Curved Dielectric Slabs and Fibers", IEEE Transactions, Microwave Theory Technology, **22** 718 (1974).

12. A. W. Snyder, L. White, D. J. Mitchell, "Radiation from Bent Optical Waveguide", Electronic Letters, **11** 332 (1974).

13. D. C. Chang, E. F. Kuester, "Surface-Wave Radiation Loss from Curved Dielectric Slabs and Fibers", IEEE Journal of Quantum Electronics, **11** 903 (1975).

14. D. Marcuse, "Curvature Loss Formula for Optical Fibers", Journal of the Optical Society of America, **66** 216 (1976).

15. D. Globe, "Weakly Guiding Fibers", Applied Optics, **10** 2252 (1971).

16. J. P. Powers, An Introduction to Fiber Optic System, (Boston: Irwin, 1993) p.20.

17. J. P. Powers, An Introduction to Fiber Optic System, (Boston: Irwin, 1993) p.72.

18. D. Marcuse, Light Transmission Optics, Second Edition, (New York: Van Nostrand Reinhold, 1982) p.481.

19. P. Green Jr., Fiber Optic Networks, (Englewood Cliffs: Prentice Hall, 1993) p.51.

20. G. P. Agrawal, Nonlinear Fiber Optics, (Boston: Academic Press, 1989) p.8.

21. G. P. Agrawal, Nonlinear Fiber Optics, (Boston: Academic Press, 1989) p.9.

22. J. P. Powers, An Introduction to Fiber Optic System, (Boston: Irwin, 1993) p.59.

23. J. P. Powers, An Introduction to Fiber Optic System, (Boston: Irwin, 1993) p.29.

24. D. Marcuse, Theory of Dielectric Optical Waveguides, Second Edition, (London: Academic Press, 1991) p.73.

25. D. Kliger, J. Lewis, C. E. Randall, Polarized Light in Optics and Spectroscopy, (San Diego: Academic Press, 1990) p.11.

26. I. P. Kaminow, "Birefringent Single-mode Fibers", Advances in Ceramics Proceeding, **2** 204 (1981).

27. N. Fürstenau, "Performance of the Double-Polarization Method in Interferometric Digital Force Sensing by Fiber Tension Bending", SPIE Polarization Consideration for Optical Systems, **891** 209 (1988).

28. T. Okoshi, K. Kikuchi, Coherence Optical Fiber Communications, (Tokyo: KTK Scientific Publisher, 1988) p.198.

29. F. M. Ernsberger, Polarized Light in Glass Research, (Pittsburgh: PPG Industries, 1970) p.44.

30. H. Mueller, "The Theory of Photoelasticity", Journal of the American Ceramics Society, 27 (1938).

31. A. Kuske, G. Robertson, Photoelastic Stress Analysis, (London: John Wiley & Sons, 1974) p.73.

32. F. M. Ernsberger, Polarized Light in Glass Research, (Pittsburgh: PPG Industries, 1970) p.46.

33. E. B. Shand, Glass Engineering Handbook, (New York: McGraw-Hill, 1958) p.58.

34. W. Primak, D. Post, "Photonics Constants of Vitreous Silica and Its Elastic Coefficient of Refractive Index", Journal of Applied Physics, **30** 779 (1959).

35. G. W. Morey, The Properties of Glass, Second Edition, (New York: Reinhold, 1954) p.442.

36. E. P. Popov, Introduction to Mechanics of Solids, (Englewood Cliffs: Prentice-Hall, 1968) p.379.

37. G. W. Morey, The Properties of Glass, Second Edition, (New York: Reinhold, 1954) p.339.

38. C. Kao, Optical Fiber Systems: Technology, Design, and Applications, (New York: McGraw-Hill, 1982) p.61.

39. I. H. Malitson, "Interspecimen Comparison of the Refractive Index of Fused Silica", Journal of the Optical Society of America, **55** 1205 (1965).

40. R. Sosman, The Properties of Silica, (New York: The Chemical Catalog Company, 1927) p.687.

41. D. A. Krohn, A. R. Cooper, "Strengthening of Glass Fibers: I, Cladding", Journal of the American Ceramic Society, **52** 661 (1969).

42. G. W. Scherer, A. R. Cooper, "Thermal Stress in Clad-Glass Fibers", Journal of the American Ceramic Society, **63** 346 (1980).

43. S. Scholes, Modern Glass Practice, (Boston: Cahners Books, 1974) p.46.

44. ABAQUS Finite Element Code, Version 6.4-1, ABAQUS Inc., Providence, Rhode Island.